Marine and Petroleum Geology 163 (2024) 106774

Contents lists available at ScienceDirect

Marine and Petroleum Geology

journal homepage: www.elsevier.com/locate/marpetgeo

Evolution of Upper Carboniferous tight sandstone reservoirs in the Ruhr and Lower Saxony basins (NW Germany) of the Central European Variscan foreland

Dennis Quandt *, Benjamin Busch, Christoph Hilgers

Institute of Applied Geosciences, Structural Geology & Tectonics, KIT – Karlsruhe Institute of Technology, Campus South, Adenauerring 20a, 76131 Karlsruhe, Germany

ARTICLE INFO

Keywords:
Upper carboniferous variscan foreland basin
Sandstone petrography
Tight gas
Diagenesis
Unroofing
Quartz cementation

ABSTRACT

Foreland basins have been extensively explored for hydrocarbon resources, geothermal, and gas storage applications, and multidisciplinarily studied to reconstruct orogenic processes. In fact, in the case of the Late Carboniferous Central European Variscan foreland basin, numerous drill cores have been recovered by the hard coal industry and comprehensive geological data sets have been made available by research. These cores and data sets provide a continuous record of the tectono-sedimentary and reservoir evolution over time. For this purpose, we have compiled petrophysical and petrographic literature data of >450 mostly tight (porosity <10%, permeability <1 mD) siliciclastic rock samples from Variscan foreland (Ruhr and Lower Saxony basin, NW Germany) and intramontane basins (Saar-Nahe basin, SW Germany) covering the complete Late Carboniferous stratigraphy. As a result, increases in mean grain size, sorting, detrital quartz, and proportion of metamorphic to sedimentary rock fragment contents, and decreases in detrital feldspar contents along the Westphalian B–C boundary are interpreted as a response to sedimentary recycling and unroofing of the Variscan hinterland due to tectonic uplift in the course of the northwestward propagating Variscan front. Thus, tectonics have a greater influence on sandstone petrography and porosity than the depositional environment. Porosity is mainly controlled by grain size and dissolution porosity. Basin-specific paleogeothermal gradients affect authigenic quartz (up to 25.0%) and chlorite (up to 7.7%) formation. Moreover, quartz cement contents <5% may stabilize the granular framework against mechanical compaction preserving porosity. With increasing quartz cement contents >5%, however, pore space is progressively clogged and the porosity preserving effect diminishes.

1. Introduction

Orogeny and crustal thickening causes subsidence in front of active thrust belts. Such foreland basins are documented worldwide throughout the geological history (Allen and Homewood, 1986 and references therein). Understanding the reservoir quality of foreland basin lithologies and its controlling factors is crucial to evaluate the hydrocarbon, geothermal, and/or storage potentials in order to minimize exploration costs (Mann et al., 2003; Edlmann et al., 2015; Banks and Harris, 2018; Worden et al., 2018). A quantified record of sandstone petrography over time enables to evaluate reservoir quality, to determine its controlling factors (e.g. Becker et al., 2017, Busch et al., 2019, Wüstefeld et al., 2017a, Quandt et al., 2022a, b, Civitelli et al., 2023, 2024, Khan et al., 2024), and to trace the tectono-sedimentary history (e.g. Dickinson and Suczek, 1979; Mack, 1984; Garzanti, 2016 and references therein, Critelli, 2018; Critelli et al., 2023; Costamagna and Criniti, 2024),

Among the different foreland basins, the Late Carboniferous Variscan foreland basin in Central Europe represents a well-studied example due to decades-long hard coal mining accompanied by comprehensive recordings of seismic reflection lines and hundreds of drilling campaigns recovering ten thousand meters of drill cores (e.g. Drozdzewski, 1993; Maynard et al., 1997; Stollhofen, 1998). In previous publications on the Variscan foreland (Ruhr and Lower Saxony basin) and intramontane (Saar-Nahe basin) basins, Late Carboniferous sandstone petrography and reservoir quality were investigated (Becker et al., 2017; Wüstefeld et al., 2017a; Busch et al., 2019; Quandt et al., 2022a, accepted, Greve et al., 2023, 2024, under review).

Here, we compile these previously published petrographical and petrophysical data and complement them with new data. The

* Corresponding author.
E-mail addresses: dennis.quandt@kit.edu (D. Quandt), benjamin.busch@kit.edu (B. Busch), christoph.hilgers@kit.edu (C. Hilgers).

https://doi.org/10.1016/j.marpetgeo.2024.106774
Received 17 January 2024; Received in revised form 26 February 2024; Accepted 26 February 2024
Available online 27 February 2024
0264-8172/© 2024 The Authors. Published by Elsevier Ltd. This is an open access article under the CC BY license (http://creativecommons.org/licenses/by/4.0/).

siliciclastic core and outcrop samples originate from intramontane (Saar-Nahe basin) and foreland basins (Ruhr and Lower Saxony basins) across the Variscan mountain belt. They cover the Late Carboniferous stratigraphy from Namurian B/C to Westphalian A-D to Stephanian A-B and thus provide a continuous and comprehensive sedimentary record. This enables gapless conclusions on tectono-sedimentary and reservoir quality evolution of the evolving Variscan foreland basin over time.

2. Geological setting

2.1. Variscan orogeny

The Devonian-Carboniferous convergence of Gondwana and Laurussia including the Armorica and Avalonia microplates separated by the Rheic ocean resulted in the closure of the Rheic ocean and the Variscan orogeny across Central Europe (e.g. Matte, 2001). The closure of the Rheic ocean produced a suture that is traceable in central and southwestern Europe (e.g. Nance et al., 2010). In the Late Carboniferous, the Variscan orogeny was accompanied by the formation of foreland basins in front of the Variscan thin-skinned fold and trust belt due to its load inducing lithospheric flexure and fault-controlled intramontane basins (Korsch and Schäfer, 1995; Opluštil and Cleal, 2007, Cleal et al., 2009, Fig. 1). The near-equatorial basin locations with widespread wetland forests, a warm-humid climate, high sedimentation rates, and up to a few km deep burial promoted the formation of extensive coal seams (Opluštil and Cleal, 2007, Cleal et al., 2009). Northwestward verging folds and decreasing metamorphic ages indicate a northwestward propagating Variscan front with its foreland basins during Late Carboniferous times (Shackleton et al., 1982; Ahrendt et al., 1983). The foreland basins show a general trend from marine to continental depositional environments during the Late Carboniferous with numerous deposits indicating marine ingressions. However, the timing of these changes are diachronous with the eastern basins experiencing these changes earlier than the western basins (Opluštil and Cleal, 2007).(Cleal et al., 2009)

2.2. Ruhr and Lower Saxony foreland basin evolution

The Ruhr basin transitions northwards into the present-day Lower Saxony basin. Ibbenbüren, Piesberg, and Hüggel are uplifted blocks in the Lower Saxony basin that show structural similarities with the Ruhr basin. They represent the northwesternmost outcrops of Late Carboniferous strata in Germany (Drozdzewski, 1993, Fig. 1). Namurian A siltstone and claystone successions lacking coal seams document a purely marine depositional environment for the Ruhr and Lower Saxony basins (Drozdzewski, 1993, Cleal et al., 2009). However, intercalated Namurian B sandstone sequences in the southern Ruhr basin already reflect the northwestward propagating Variscan front (Drozdzewski, 1993). Consequently, the marine influence declined during the Namurian B–C and the depositional environment transitioned into a marine delta to lower delta plain setting where peat was deposited representing the first coal seams of the Ruhr basin. The Lower Saxony basin shows similar siltstone and claystone sequences. Intercalated fluvial sandstones point to a partly terrestrial depositional environment during late Namurian times (Cleal et al., 2009). Sediments originated from the Variscan mountains in the south. Additional sediment sources are metamorphosed sandstones of Devonian age derived from Baltica and accreted to the Rhenohercynian (Franke and Dulce, 2017; Franke et al., 2019). The Variscan tectono-stratigraphic Rhenohercynian unit represents a fold and thrust belt adjacent to the Variscan foreland basin (Oncken et al., 1999). The input of Baltica-derived sediments decreases from Namurian A to C (Franke et al., 2019).

In Westphalian A to B times, subsidence and coal formation culminated in the Ruhr area. Fining and coarsening upward siliciclastic successions in the Ruhr basin indicate deposition in prodelta, lower and upper delta plains (Greve et al., 2023), while upward fining siliciclastic rock sequences in the Lower Saxony basin point to fluvial deposition (Quandt et al., 2022a). The Namurian northward transport direction of sediments persisted throughout the Westphalian and the input of accreted metasediments from Baltica increased again (Franke and Dulce, 2017; Franke et al., 2019).

In the course of the multiple tectonic phases in the late Westphalian, the Variscan orogen was folded, inverted, and uplifted (Corfield et al., 1996; Maynard et al., 1997; Jones and Glover, 2005, Cleal et al., 2009).

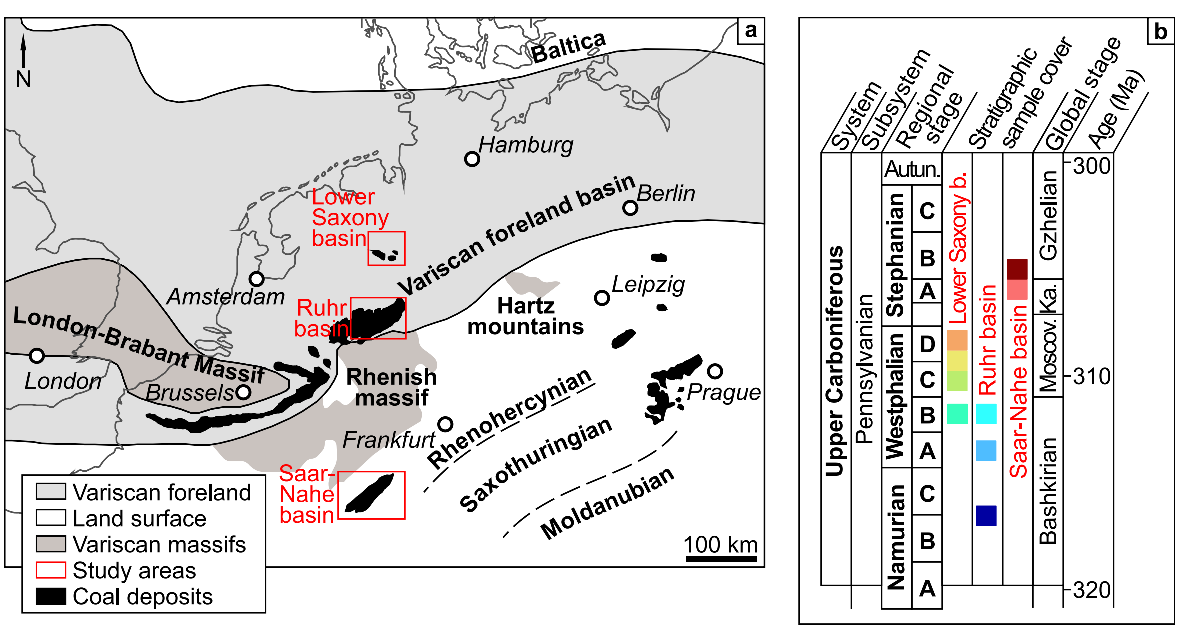

Fig. 1. (a) Simplified paleogeographic map of Central Europe during the Late Carboniferous (modified after Quandt et al., 2022a and references therein). (b) Stratigraphic column for the Upper Carboniferous (modified after Lucas et al., 2022). From north to south, the Lower Saxony basin, Ruhr basin, and Saar-Nahe basin cover the Namurian B/C, Westphalian A-D, and Stephanian A-B stratigraphy. These regional stages overlap with the global stages Bashkirian (Namurian A-C and Westphalian A-B), Moscovian (Moscov., Westphalian C-D), Kasimovian (Ka., Stephanian A), and Gzhelian (Stephanian B–C and Autunian, Autun.).

As a consequence, a rain shadow to the north of the orogeny probably constituted, climate conditions changed from humid to semi-arid, and the extent of coal swamps decreased (Roscher and Schneider, 2006; Schneider et al., 2020; Dusséaux et al., 2021). Moreover, red beds and perennial river deposits became progressively more prominent in the geological record of the Ruhr and Lower Saxony basin (Drozdzewski, 1993; Jones and Glover, 2005). This fluvial deposition continued throughout the Westphalian in the Lower Saxony basin and resulted in grain coarsening (Jones and Glover, 2005; Becker et al., 2017; Wüstefeld et al., 2017a; Busch et al., 2019; Quandt et al., 2022a). Sediments were supplied from the south with Variscan mountain sources dominating over Baltica-derived metasediments accreted to the Rhenohercynian (Maynard et al., 1997; Franke et al., 2019). The progressive northwestward propagation of the Variscan front culminating in Stephanian A (Cleal et al., 2009) and increasingly arid climate conditions terminate peat formation in the German foreland basins in Westphalian C to D (Drozdzewski, 1993).

2.3. Intramontane Saar-Nahe basin evolution

The Saar-Nahe basin constitutes a fault-controlled intramontane molasse basin (Korsch and Schäfer, 1995). Its formation has been associated with dextral strike-slip faulting generating a transtensional basin and, contrastingly, attributed to Variscan thrust fault reactivation (e.g. Korsch and Schäfer, 1991; Henk, 1993; Schäfer, 2011). Folding was interpreted as differential subsidence (Henk, 1993).

Late Namurian conglomerates and fining upward sandstones represent the earliest sedimentary fill in the Saar-Nahe basin (Korsch and Schäfer, 1995). They have been associated with an alluvial fan or fluvial depositional environment and correspond to the proto-rift phase that continues into the Westphalian (Schäfer and Korsch, 1998; Stollhofen, 1998).

The Westphalian A-C is characterized by fluvial depositional environments that transition into deltaic depositional environments in Westphalian C-D (Schäfer and Korsch, 1998; Schäfer, 2011). These deltas are associated with intramontane freshwater lakes indicated by limestones, algal laminites, and ostracods (Stollhofen, 1998). The basin was fed by braided and meandering rivers transporting sediments from the Rhenish Massif southwards (Schäfer, 2011). The Westphalian sedimentary rock record documents the proto-rift phase of the Saar-Nahe basin (Stollhofen, 1998; Schäfer, 2011). While coals seams are absent in Westphalian A strata, their abundance increases in Westphalian B-D strata (Schäfer, 2011).

From the Westphalian to the Stephanian and Early Rotliegend, the climate progressively changes to semi-arid conditions, the source area shifts from the northern Rhenish Massif to the southern Black Forest, Vosges and Massif Central, and deltaic depositional environments become dominant (Schäfer, 2011). Stephanian coarsening upward siliciclastic successions represent the pre-volcanic syn-rift phase. The Early Rotliegend constitutes the onset of the volcanic syn-rift phase, which transitions into the post-rift phase in the Late Rotliegend (Stollhofen, 1998).

3. Methods

3.1. Data compilation

This study comprises quantified petrography (354 samples), porosity, and permeability data (441 samples) of overall >450 samples from >1900 m cored intervals and surface outcrops compiled from literature (Becker et al., 2017; Wüstefeld et al., 2017a; Busch et al., 2019; Quandt et al., 2022a, accepted; Greve et al., 2023, 2024, under review) and complemented by new data (Table 1). The data sets stratigraphically belong to the Namurian B-C, Westphalian A-D, and Stephanian A-B (Becker et al., 2017; Wüstefeld et al., 2017a; Busch et al., 2019; Franke et al., 2019; Quandt et al., 2022a, accepted; Greve et al., 2023, 2024, under review). The regional Upper Carboniferous stratigraphy used in western Europe and consistently applied here is equivalent to the Pennsylvanian, which is subdivided into the Bashkirian (Namurian A-C and Westphalian A-B), the Moscovian (Westphalian C-D), the Kasimovian (Stephanian A) and the Gzhelian (Stephanian B–C) stages (Lucas et al., 2022).

Table 1
Summary of the data sets presented in this study.

Study area	Drill core/sample location	Coordinates (WGS84)	Sample type	Logged core interval (m)	Number of samples	Stratigraphy	Reference
Saar-Nahe basin	Primsweiler-1	N 49.397089 E 6.848970	Drill core	28.61	24	Stephanian A-B	Quandt et al. (accepted)
Lower Saxony basin	Woitzel	N 52.313932 E 7.701347	Outcrop	/	29	Westphalian D	Becker et al. (2017)
	Hüggel	N 52.217744 E 7.973585	Outcrop	/	11	Westphalian D	Becker et al. (2017)
	Piesberg	N 52.319469 E 8.016068	Outcrop	/	51	Westphalian C/D	Wüstefeld et al. (2017a)
	Well A	Confidential	Drill core	120.00	43	Westphalian C-D	Busch et al. (2019)
	Well B	Confidential	Drill core	308.00	51	Westphalian C-D	Busch et al. (2019)
	Zeche Ibbenbüren	N 52.290566 E 7.738472	Drill core	322.20	80	Westphalian B–C	Quandt et al., (2022a), this study
Ruhr basin	Haidberg-1	N 51.726451 E 7.136701	Drill core	295.50	37	Westphalian B	Greve et al. (2023, under review)
	Pelkum-1	N 51.627513 E 7.736707	Drill core	533.55	61	Westphalian A	Greve et al. (2023, 2024)
	Bork-1	N 51.671468 E 7.488589	Drill core	307.40	42	Westphalian A	Greve et al. (2023, under review)
	Quarry Külpmann	N 51.373513 E 7.311732	Outcrop	/	16	Namurian C	This study
	Quarry Rauen	N 51.423376 E 7.355875	Outcrop	/	9	Namurian C	This study
	Harkortsattel	N 51.390052 E 7.383876	Outcrop	/	2	Namurian B/C	This study

Exact stratigraphy of Harkortsattel and Piesberg samples is unclear. They belong to the Namurian B and/or C and Westphalian C and/or D, respectively.

3.2. Data comparability

Detailed descriptions of methods are given in the respective papers cited in this study (Becker et al., 2017; Wüstefeld et al., 2017a; Busch et al., 2019; Quandt et al., 2022a, accepted; Greve et al., 2023, 2024, under review). Porosity and permeability of all samples presented in this study were measured on dried (at ≥40 °C over two days) cylindrical one-inch diameter rock plugs. For reasons of cylindricality, plug ends were trimmed and used for thin section production. Porosity of all samples was consistently determined with a semi-automated micromeritics Accupyc II 1340 helium pycnometer. Permeability was measured with an isostatic flow cell (Becker et al., 2017; Wüstefeld et al., 2017a) or a Westphal Mechanik air permeameter (Busch et al., 2019; Quandt et al., 2022a, accepted; Greve et al., 2023, 2024, under review). In both approaches, permeability was Klinkenberg-corrected (Klinkenberg, 1941; Rieckmann, 1970). Detection limit of the Westphal Mechanik air permeameter is 0.0001 mD. Different confining pressures of 1.2, 2, 3, 20, and 30 MPa applied during measurements (Becker et al., 2017; Wüstefeld et al., 2017a; Busch et al., 2019; Quandt et al., 2022a, accepted; Greve et al., 2023, 2024, under review) required a correction to a confining pressure of 2 MPa using equation (1) after David et al. (1994).

$$k = k_0 \times e^{-\gamma\left(P_{eff}-P_0\right)} \tag{1}$$

k is the permeability corrected for a consistent confining pressure P_{eff} of 2 MPa, K_0 is the permeability measured at the confining pressure P_0 applied at the respective measurement, and γ is the pressure sensitivity coefficient of 0.03 MPa^{-1} derived by Becker et al. (2017).

Mean sample grain size, skewness, and sorting (Folk and Ward, 1957) were consistently calculated based on 100 grains per sample using image analysis software (Becker et al., 2017; Wüstefeld et al., 2017a; Busch et al., 2019; Quandt et al., 2022a, accepted; Greve et al., 2023, 2024, under review). Sample petrography was consistently quantified in oriented thin sections using a transmitted light microscope connected to a Pelcon semi-automatic point counting stage (Becker et al., 2017; Wüstefeld et al., 2017a; Busch et al., 2019; Quandt et al., 2022a, accepted; Greve et al., 2023, 2024, under review). 300 points per sample were counted and each attributed to a category (Table A in appendix).

Sandstone composition was determined using three ternary plots. First, detrital quartz, detrital feldspar, and rock fragment contents were normalized to each other and plotted in a ternary QFR (quartz, feldspar, rock fragments) diagram after Folk (1980). Second, depositional detrital feldspar contents before diagenetic dissolution and/or mineral transformation were recalculated based on contents of total detrital feldspar, minerals replacing feldspar (clay, carbonate, chlorite), and secondary porosity due to dissolution. Since replacements and dissolutions may also be related to rock fragments, this recalculation represents a maximum estimate on depositional feldspar content. Detrital quartz, depositional detrital feldspar, and rock fragment contents were normalized to each other and plotted in a ternary QFR diagram after Folk (1980). Third, normalized contents of sedimentary (SRF), igneous (IRF), and metamorphic rock fragments (MRF) were plotted in a ternary diagram similar to Critelli and Le Pera (1994).

In order to ensure comparability of the point counting data sets collected by different authors, point counting data were reassessed using available thin sections from publications cited. Point counting categories were subsequently merged as follows (Table A in appendix). Detrital K-feldspar and plagioclase are given as total detrital feldspar. All carbonate (i.e. ankerite, siderite, (Fe-) calcite, and (Fe-) dolomite) and clay (illite and kaolinite) cements were each combined in a single category. Similarly, carbonate and clay minerals replacing feldspar or rock fragments are each summarized in a single category. Opaque components comprise coal and ore minerals. Claystone, siltstone, and sandstone fragments are classified as siliciclastic rock fragments. Phyllite rock fragments comprise all schistose rock fragments such as slates and schists. Pseudomatrix, rip up clasts, paleosol, and their replacements are summarized as pseudomatrix. Pseudomatrix, detrital muscovite, detrital chlorite, shale and phyllite rock fragments constitute ductile component contents. Accessory titanite, tourmaline, zircon, and rutile are grouped as heavy minerals.

On the basis of the reassessed point counting results, compaction porosity loss (COPL), cementation porosity loss (CEPL), ICOMPACT, and intergranular volume (IGV) were recalculated according to equations (2)–(5), respectively (Lundegard, 1992; Paxton et al., 2002).

$$COPL = P_i - (((100 - P_i) \times P_{mc}) / (100 - P_{mc})) \text{ with } P_{mc} = P_o + C \tag{2}$$

$$CEPL = (P_i - COPL) \times C / P_{mc} \tag{3}$$

$$ICOMPACT = COPL/(COPL + CEPL) \tag{4}$$

$$IGV = Intergranular\ pore\ space + Intergranular\ cements + Depositional\ matrix \tag{5}$$

COPL and CEPL are a function of the initial porosity P_i, total optical porosity P_o, minus cement porosity P_{mc}, and total pore-filling cement C. P_{mc} is the sum of P_o and C (Lundegard, 1992). Calculations of COPL and CEPL were consistently performed with an initial porosity of 45%, typical for fluvial sediments (Lundegard, 1992). ICOMPACT values > 0.5 are COPL-dominated and ICOMPACT values < 0.5 are CEPL-dominated (Lundegard, 1992).

4. Results

4.1. Petrography

4.1.1. Texture

Mean sample grain sizes range from 0.006 mm (very fine silt) to 1.35 mm (coarse sand, Fig. 2a). Namurian B/C to Westphalian C samples are characterized by P75 mean grain sizes of 0.4 mm (i.e. 75% of samples have a mean grain size <0.4 mm) with Westphalian A and B (Ruhr) samples being the finest. Westphalian C samples mark an increase in mean sample grain size that culminates in P25 mean sample grain size of >0.3 mm in Westphalian D (i.e. 75% of samples have a mean grain size >0.3 mm). Except for two outliers, mean sample grain sizes <0.11 mm lack in the Westphalian C-D. Stephanian A-B samples show mean grain sizes consistently <0.3 mm.

Sorting coefficients vary from 0.4 to 1.6 (Fig. 2b). Between Namurian B/C and Westphalian B (Ruhr), mean sorting coefficients slightly increase from 0.6 to 0.7 equivalent to moderately to moderately well sorted samples. Westphalian C samples mark a decreasing trend in mean sorting coefficient from 0.6. to 0.5 in Westphalian D, which is interrupted by a mean sorting coefficient of 0.8 in Westphalian C/D. Stephanian A-B samples have mean sorting coefficients >0.9 corresponding to poorly sorted samples.

Skewness coefficients range from −0.35 to 0.43 (Fig. 2c). Namurian B/C to Westphalian B samples show a decrease in mean skewness coefficients from 0.2 to 0.1. From Westphalian C to D, the mean skewness coefficient remains constant and negative skewness coefficients become increasingly prominent. Stephanian A-B samples show mean skewness coefficients >0.15.

4.1.2. Detrital mineralogy

Quartz, rock fragments, and feldspar are the major detrital mineralogical components of the sample set (Fig. 2d–g). Mean and median detrital quartz contents decrease from 51-53% in Namurian B/C to predominantly 39–42% in Westphalian A and B (Fig. 2d). Westphalian C samples marks an increase in mean and median detrital quartz contents to >50% that remains constant throughout the Westphalian C/D and D. These ranges are covered by Stephanian A-B samples, which have the highest mean detrital quartz contents consistently >55%.

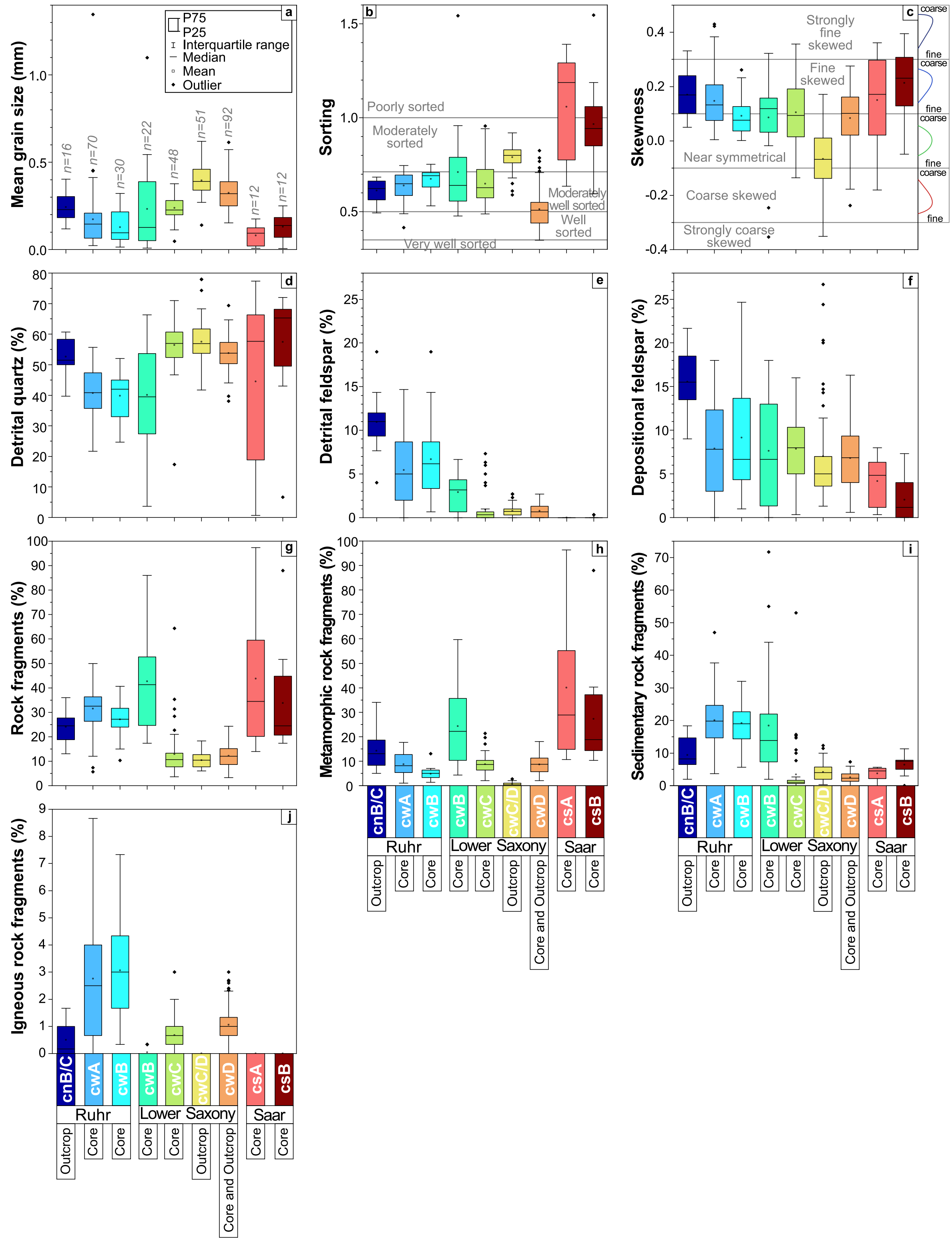

Fig. 2. Box plots of textural features and detrital mineralogy. Evolution of (a) mean grain size, (b) sorting, (c) skewness, (d) detrital quartz content, (e) detrital feldspar content, (f) recalculated depositional feldspar content, (g) rock fragments content, (h) metamorphic rock fragments content, (i) sedimentary rock fragments contents, and (j) igneous rock fragments content over time. Data were compiled from literature (Becker et al., 2017; Wüstefeld et al., 2017a; Busch et al., 2019; Quandt et al., 2022a, accepted; Greve et al., 2023, 2024, under review) and complemented by new data. Namurian B/C (cnB/C), Westphalian A-D (cwA-D), and Stephanian A-B (csA-B) are abbreviated. For legend of box plots see Fig. 2a. Unless otherwise indicated, number of samples *n* used to calculate box plots are given in Fig. 2a.

Mean detrital feldspar contents almost progressively decrease from 11% in Namurian B/C to <1% in Westphalian C to D (Fig. 2e). Stephanian A-B samples are feldspar-free except for a few point counts (0–0.33% per sample). Recalculation of depositional feldspar contents results in an approximation of contents without completely diminishing the general negative trend over time (Fig. 2f).

P25 contents of total rock fragments increase from 19% in Namurian B/C to ≥24% in Westphalian A and B (Fig. 2g). Westphalian C samples mark a decrease in rock fragment contents (P75 < 16%) that remains constant until Westphalian D. Stephanian A-B samples show the highest P25 rock fragment contents ≥20%.

Rock fragments are subdivided into metamorphic, sedimentary and igneous. Mean metamorphic rock fragment contents decrease from Namurian B/C (13%) to Westphalian B (Ruhr, 5%, Fig. 2h). Westphalian B (Ibbenbüren) show and increase in metamorphic rock fragments to up to 60%. Westphalian C-D samples have metamorphic rock fragment contents in the range of Westphalian A samples. Stephanian A-B have consistently >10% metamorphic rock fragments constituting the highest contents.

P75 of total sedimentary rock fragments increase from 15% in Namurian B/C to ≥22% in Westphalian A and B (Fig. 2i). Westphalian C samples mark an abrupt decrease in sedimentary rock fragment contents to values consistently ≤10% (except for some outliers) that remains constant throughout Westphalian D. Stephanian A-B samples have similar contents (≤11%).

Westphalian A and B (Ruhr) samples reveal major peaks in total igneous rock fragment contents of up to 8.7%. The other samples bear 0–3% igneous rock fragments (Fig. 2j).

Taken together, Namurian B/C to Westphalian B samples are predominantly classified as feldspathic litharenite and litharenite, while Westphalian C to Stephanian B samples are mainly litharenites and sublithic arenites (Fig. 3a). Considering the recalculated depositional feldspar contents, samples shift toward subarkose and lithic arkose compositions (Fig. 3b).

The proportion of normalized metamorphic and sedimentary rock fragments shows a change between Westphalian B and C (Fig. 3c). Namurian B/C to Westphalian B rock fragments are dominantly sedimentary, whereas Westphalian C-D samples are dominantly metamorphic. Westphalian C/D samples constitute an exception.

Accessory detrital minerals comprise muscovite (0–17.3%), opaques (0–8.7%), heavy minerals (titanite, tourmaline, zircon, and rutile, 0–3.7%), chlorite (0–2.3%), and biotite (0–1.0%) in order of decreasing mean contents. Muscovite contents are highest in Westphalian A to B samples with up to 17.3% per sample (Fig. 4a). Westphalian C to D samples have the lowest muscovite contents (P75 < 2%). A similar trend is observed for the content of ductile components (i.e. pseudomatrix, shale and phyllite rock fragments, and detrital muscovite and chlorite) that shows maximum values up to 78.3% in Westphalian A-B samples and P75 < 20% in Westphalian C to D samples (Fig. 4b). Stephanian A to B samples show ranges comparable with Westphalian B to C samples. Total heavy mineral contents show no systematic variation in content over time (Fig. 4c). Elevated heavy mineral contents >1% per sample are observed among Westphalian A, C, and particularly D samples.

4.1.3. *Authigenic mineralogy*

In order of decreasing mean contents, authigenic cement phases in primary pore space comprise syntaxial quartz (0–19.0%), carbonate (calcite, dolomite, siderite, ankerite, 0–38.3%), clay (illite, kaolinite, 0–12.3%), pore-lining and pore-filling Fe-hydroxides (0–15.7%), chlorite (0–7.7%), barite and other sulfates (0–6.7%), and feldspar (0–0.3%). Namur B/C to Westphalian B samples have P75 pore-filling (primary pore space) cement contents <7% (Fig. 4d). Westphalian C to D samples show an increase with P25 pore-filling cement contents ≥12% including the highest quartz (up to 25%) and clay (up to 12%) cement contents (Fig. 4e and f). Similarly, the highest carbonate cement contents are observed among Westphalian C and D samples (Fig. 4g). Stephanian A-B samples are characterized by total pore-filling cement contents consistently <5%. Authigenic chlorite (i.e. chlorite cement and chlorite replacing component) is particularly present in Westphalian C-D samples with contents up to 7.7%, whereas Westphalian A-B samples are devoid of authigenic chlorite (Fig. 4h). In addition, secondary pore space such as fractures and dissolved components are filled with calcite, siderite, or sulfides. Clay minerals (0–12.0%) and carbonate minerals (0–7.0%) replace feldspar and rock fragments. Chlorite replaces feldspar, rock fragments, and kaolinite (0–0.3%).

4.1.4. *Optical porosity*

P75 of total optical porosity is consistently <5.3% (Fig. 5a). Outliers of up to 26.7% optical porosity belong to Westphalian C/D samples. Secondary porosity related to dissolution (0–26.7% per sample)

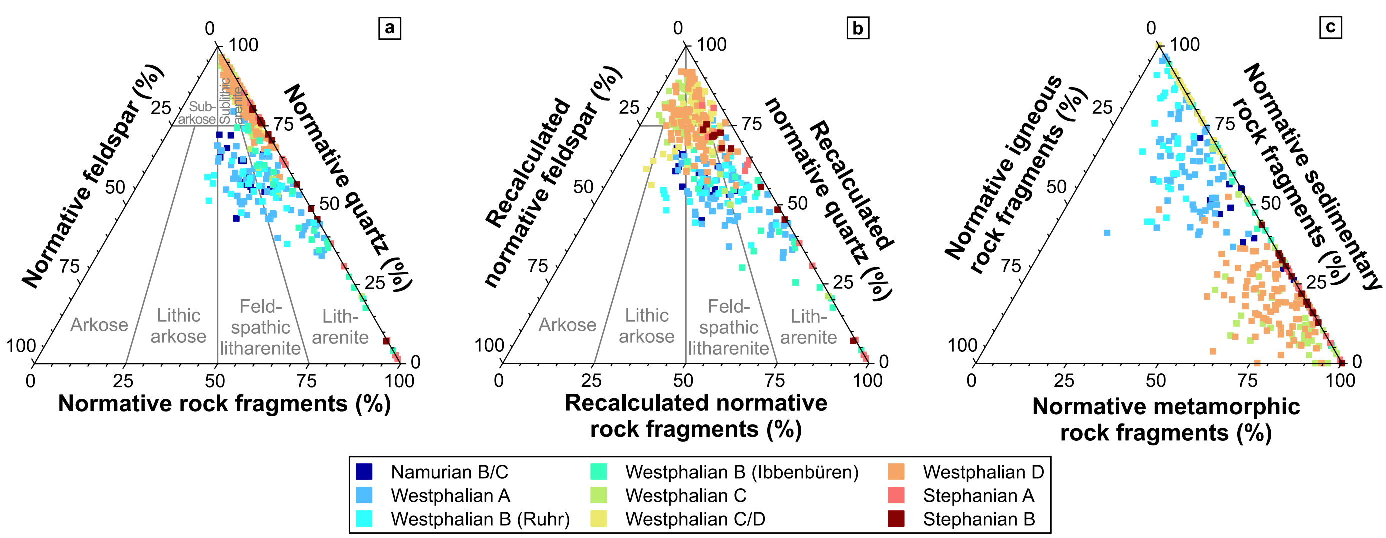

Fig. 3. Ternary classification diagrams for sandstones after Folk (1980). (a) Normalized contents of detrital quartz, feldspar and rock fragments (QFR), (b) QFR based on recalculated depositional feldspar contents and corresponding recalculated normative detrital quartz and rock fragment contents, and (c) normalized contents of igneous, sedimentary, and metamorphic rock fragments. See methods for calculation of normalized contents and recalculated depositional feldspar contents. In addition to sandstones, also siltstones are considered in the plots. Data were compiled from literature (Becker et al., 2017; Wüstefeld et al., 2017a; Busch et al., 2019; Quandt et al., 2022a, accepted; Greve et al., 2023, 2024, under review) and complemented by new data.

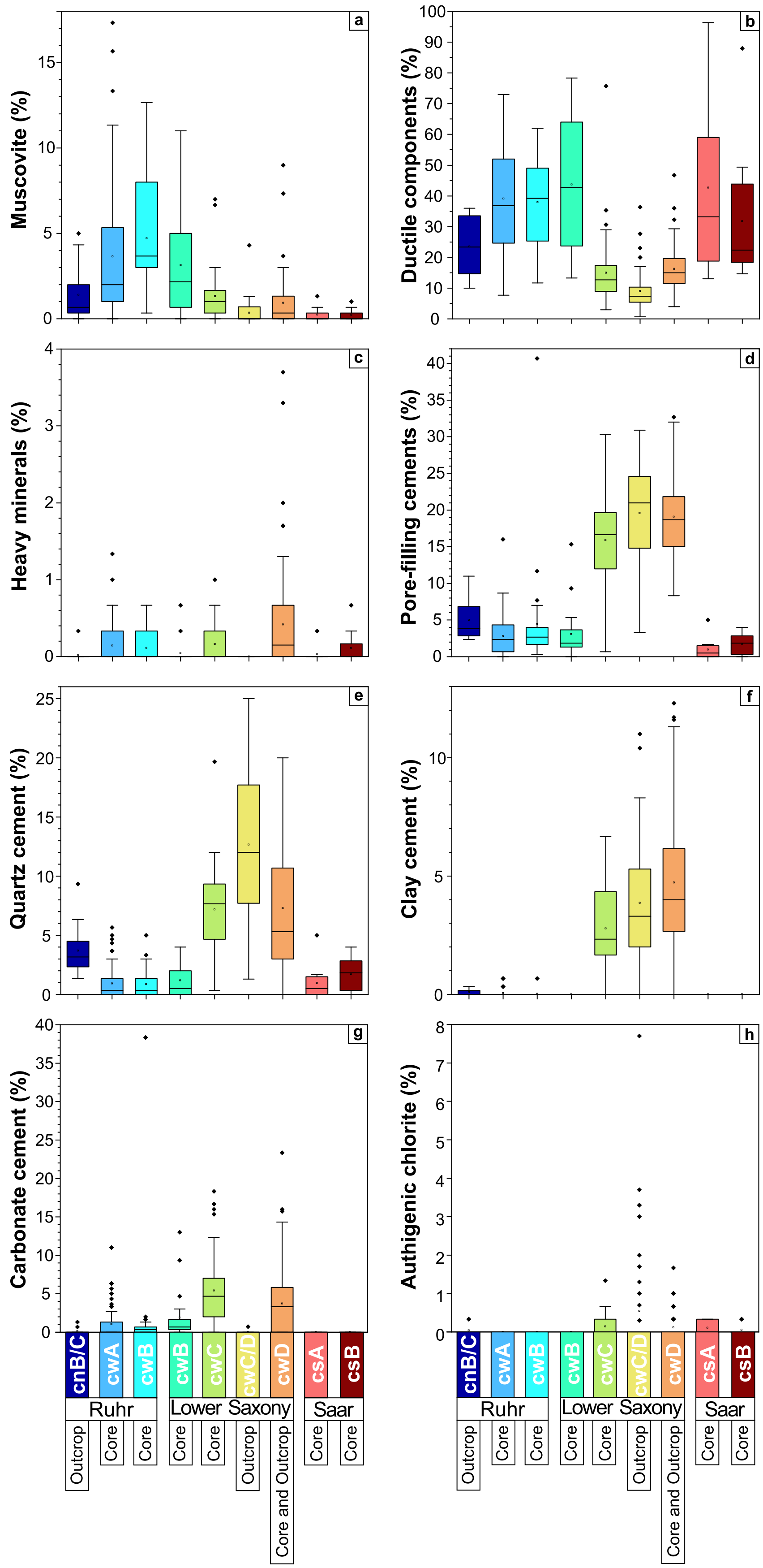

(caption on next page)

Fig. 4. Box plots of accessory detrital and authigenic minerals. Evolution of (a) detrital muscovite contents, (b) ductile component contents (i.e. pseudomatrix, rip up clasts, paleosol, shale and phyllite rock fragments, detrital muscovite and chlorite), (c) heavy mineral contents (i.e. titanite, tourmaline, zircon, and rutile), (d) total pore-filling cement contents, (e) quartz cement contents, (f) clay cement contents, (g) carbonate cement contents, and (h) authigenic chlorite contents over time. Data were compiled from literature (Becker et al., 2017; Wüstefeld et al., 2017a; Busch et al., 2019; Quandt et al., 2022a, accepted; Greve et al., 2023, 2024, under review) and complemented by new data. Namurian B/C (cnBC), Westphalian A-D (cwA-D), and Stephanian A-B (csA-B) are abbreviated. For legend of box plots see Fig. 2a. Unless otherwise indicated, number of samples *n* used to calculate box plots are given in Fig. 2a.

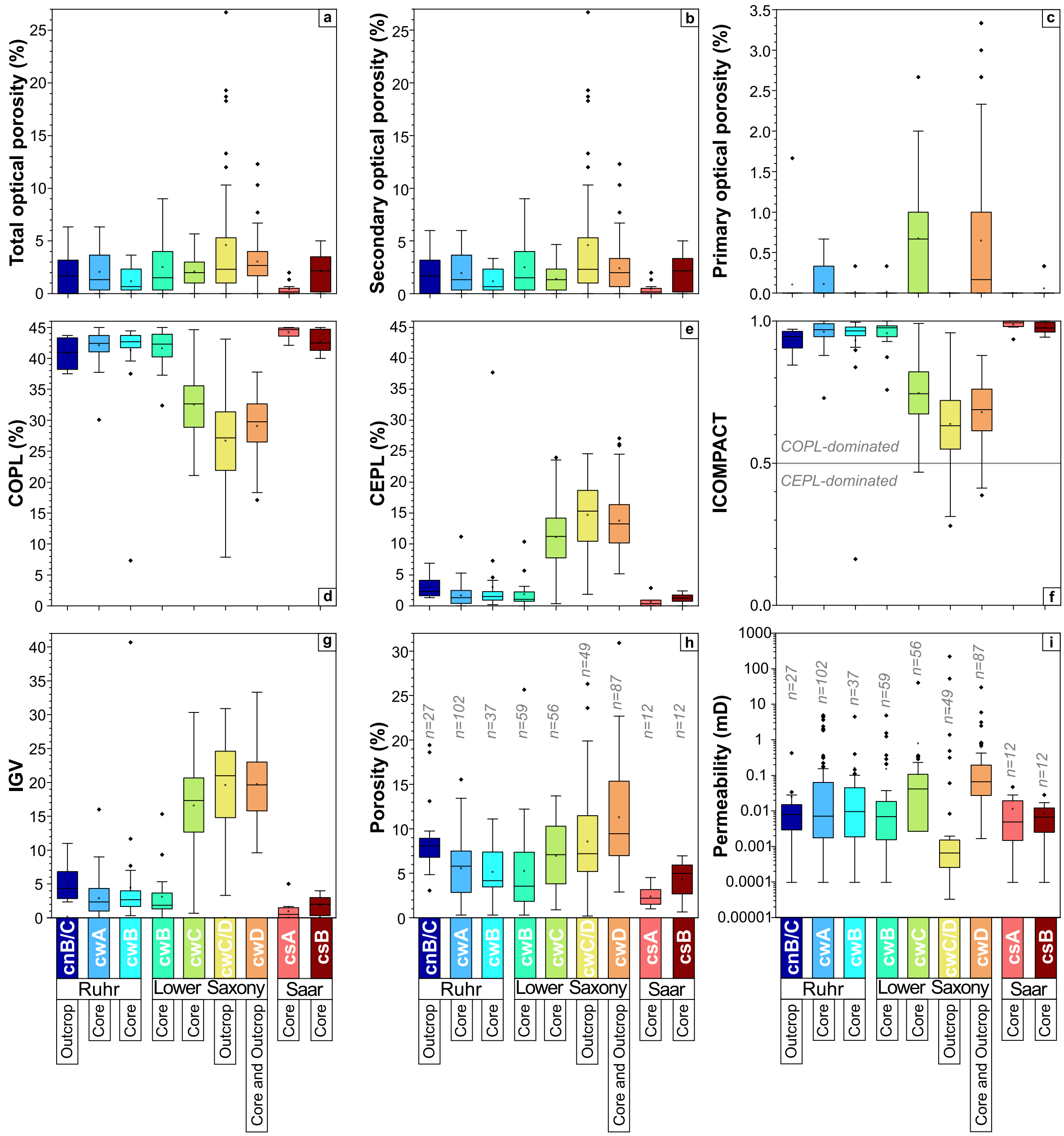

Fig. 5. Box plots of porosity, permeability, and compaction values. (a) Total optical porosity, (b) secondary porosity, (c) primary porosity, (d) COPL, (e) CEPL, (f) ICOMPACT, (g) intergranular volume (IGV), (h) porosity, and (i) permeability over time. Data were compiled from literature (Becker et al., 2017; Wüstefeld et al., 2017a; Busch et al., 2019; Quandt et al., 2022a, accepted; Greve et al., 2023, 2024, under review) and complemented by new data. Namurian B/C (cnBC), Westphalian A-D (cwA-D), and Stephanian A-B (csA-B) are abbreviated. For legend of box plots see Fig. 2a. Unless otherwise indicated, number of samples *n* used to calculate box plots are given in Fig. 2a.

dominates over primary (intergranular) porosity (0–3.3% per sample, Fig. 5b and c). Fractures contribute 0–1.0% per sample to total optical porosity. Westphalian C/D samples are characterized by the highest secondary porosity values of up to 26.7%, whereas all other samples have P75 secondary porosity values < 4%.

4.1.5. Compaction

Namurian B/C to Westphalian B samples have COPL values consistently >37% except for some outliers (Fig. 5d). Westphalian C to D samples mark a decrease in COPL to P75 COPL values < 36%. Stephanian A-B samples show COPL values > 40%. Consequently, P75 CEPL values of Namurian B/C and Westphalian A-B samples are <5%

(Fig. 5e). Westphalian C-D samples mark an increase in P25 CEPL values to >8%. Stephanian A-B samples show CEPL values consistently <3%.

Namurian B/C to Westphalian B samples have P25 ICOMPACT values > 0.9 (Fig. 5f). Westphalian C-D samples are characterized by P75 ICOMPACT values < 0.8 with some values < 0.5.

P75 IGV values of Namurian B/C to Westphalian B samples are <7% (Fig. 5g). Westphalian C-D samples are characterized by P25 IGV values > 12%. Stephanian A-B samples have IGV values consistently <5%.

4.2. Petrophysics

Porosity values vary between 0.2 and 30.9% (Fig. 5h). From Namurian B/C (8.1%) to Westphalian B (3.5%), mean porosity values progressively decrease and then progressively increase from Westphalian C (7.1%) to Westphalian D (9.5%, Fig. 5h). Stephanian A-B samples have the lowest mean porosity values (<6.9%).

Permeability values corrected to 2 MPa confining pressure range from below detection limit to 219.13 mD (Fig. 5i). Namurian B/C to Westphalian C samples are characterized by similar mean permeability values between 0.007 and 0.01 mD. From Westphalian C to D, mean permeability values increase to 0.06 mD except for Westphalian C/D samples that interrupt this trend due to permeability values consistently <0.002 mD except for some outliers. Stephanian A-B samples have permeability values consistently <0.05 mD.

4.3. Correlations of petrographic and petrophysical data

With increasing secondary porosity and mean grain size, porosity increases, whereas permeability shows no systematic variation (Fig. 6a and b). Outcrop samples reveal 5 to 10 percentage points higher porosity values than drill core samples but no variation in permeability (Fig. 6a). Mean sample grain sizes of the whole sample set constitute a positive correlation with detrital quartz content ($R^2 = 0.3$, Fig. 6c) and a negative correlation with ductile component content ($R^2 = 0.4$, Fig. 6d). Ductile component content in turn shows negative correlations with IGV ($R^2 = 0.5$, Fig. 6e), quartz cement content ($R^2 = 0.4$, Fig. 6f), and porosity ($R^2 = 0.2$, Fig. 6g). Westphalian B (Ruhr and Ibbenbüren) and Stephanian B samples have quartz cement contents up to 5% that are positively correlated with porosity ($R^2 > 0.5$, Fig. 6h).

5. Discussion

5.1. Geological evolution

Predominantly positive sorting and skewness coefficients between 0.4 and 1.6 (Fig. 2b and c) are typical for fluvial deposits (e.g. Friedman, 1961; McLaren, 1981; Becker et al., 2017; Wüstefeld et al., 2017a; Busch et al., 2019; Quandt et al., 2022a, accepted). Decreasing mean skewness coefficients from Namurian B/C to Westphalian B and negative skewness coefficients becoming more prominent from Westphalian B onwards possibly point to a winnowing effect that selectively removed finer grain size fractions (e.g. Duane, 1964; McLaren, 1981). Removal may be driven by fluvial or wave action as well as eolian processes, which became increasingly important toward the Early Permian (Opluštil and Cleal, 2007). The removal of finer grain size fractions indicated by the trend in skewness temporally coincides with an increase in mean grain size, a lack of mean grain sizes <0.11 mm except for one outlier, and an improvement in sorting (i.e. decreasing mean sorting coefficients except for Westphalian C/D samples, Fig. 2a and b). Among these three trends, the trend in mean grain size is the most significant one. The mean grain size trend is accompanied by changes in the mineralogical composition that cannot be explained by sediment winnowing.

Instead, the petrographic variations observed along the Westphalian B–C boundary imply a critical point in the tectono-sedimentary evolution of the Variscan foreland and hinterland. Along the Westphalian B–C boundary, mean grain size and detrital quartz content increase (Fig. 2a–d), whereas detrital feldspar, total rock fragment, sedimentary rock fragment, detrital muscovite, and total ductile component contents decrease (Fig. 2e–g, i, 4a-b). Some of these petrographic features are mutually dependent. With increasing grain size, detrital quartz contents increase and total ductile component contents decrease (Fig. 6c and d). This highlights the impact of grain size.

Petrographic characteristics of Westphalian B (Ibbenbüren) fluvial samples resemble rather Westphalian B (Ruhr) deltaic samples than the younger Westphalian C-D fluvial samples (e.g. Fig. 2d–g). Westphalian B (Ibbenbüren) samples also show a transition between stratigraphic older and younger data sets (e.g. Fig. 2a–e, f). Furthermore, deltaic samples from the Ruhr basin (Namurian B/C-Westphalian B) are occasionally characterized by large textural and mineralogical variations covering the variations observed among Westphalian B-D fluvial samples from the Lower Saxony basin (e.g. Fig. 2a, d-e). Therefore, the deltaic and fluvial samples cannot be clearly distinguished based on petrography but trends over time clearly exist. This means that tectonics probably exerted a greater control on sandstone petrography than the depositional environment, which is in turn a function of tectonics.

Changes in sandstone petrography have been qualitatively described for the Variscan foreland basin (e.g. Jones and Glover, 2005) and observed elsewhere such as in Taiwan (e.g. Dorsey, 1988) and in the Himalaya (e.g. DeCelles et al., 2014). They have been interpreted as a consequence of changing source areas and/or unroofing (e.g. Dorsey, 1988; Garzanti et al., 2004; DeCelles et al., 2014; Nagel et al., 2014; Critelli et al., 2023; Critelli and Criniti, 2021; Criniti et al., 2023). However, unroofing models proposed for the Late Carboniferous Variscan foreland have not been substantiated with large quantified petrographic data sets as presented here.

In general, the petrographic changes observed may have been caused by progressive (1) unroofing of the Variscan orogen, (2) changing source areas, (3) variations in transport distance, and/or (4) sediment recycling.

5.1.1. Unroofing of the variscan orogeny

Folding and thrusting results in uplift of continental crust. Consequently, erosion will progressively expose deeper lithostratigraphic levels. This unroofing process may result in a change in rock fragment types over time recorded in the basin lithology. The thin-skinned nature of the fold and thrust belt implies no involvement of deep, high-grade metamorphic rocks (Meissner et al., 1981; Behr et al., 1984). Instead, the Variscan fold and thrust belt, as represented by the Rhenish massif and Harz mountains, is composed of (meta-) sedimentary rocks covering low-grade metamorphic rocks and a few igneous intrusions (Franke and Dulce, 2017; Franke et al., 2019). This is in agreement with the increasing proportion of metamorphic to sedimentary rock fragments over time (Fig. 3c), the scarcity in igneous rock fragments, and the consistent lack of any rock fragments and heavy minerals indicative of high-grade metamorphism (e.g. blueschist facies and higher) in this study. However, the decreasing trends in detrital feldspar and recalculated detrital feldspar contents (Fig. 2e and f) cannot be explained by unroofing. Variations in heavy mineral contents may be indicative of unroofing (Garzanti et al., 2006; Garzanti, 2019), but no systematic variation over time was observed (Fig. 4c). Additionally, the thin-skinned tectonic structure of the source areas composed of homogenous (meta-) sedimentary rock sequences (Franke and Dulce, 2017; Franke et al., 2019) probably prevents any remarkable variation in heavy minerals.

5.1.2. Changing source areas

The Late Carboniferous Variscan foreland basin was fed by sediments from the south. Potential source areas are the Rhenish massif, Harz mountains, and accreted Baltica-derived rocks (Franke and Dulce, 2017; Franke et al., 2019). They are similarly composed of siliciclastic and low-grade metamorphic rocks (up to greenschist facies, Ahrendt et al., 1983; Behr et al., 1984; Franke and Dulce, 2017; Franke et al., 2019).

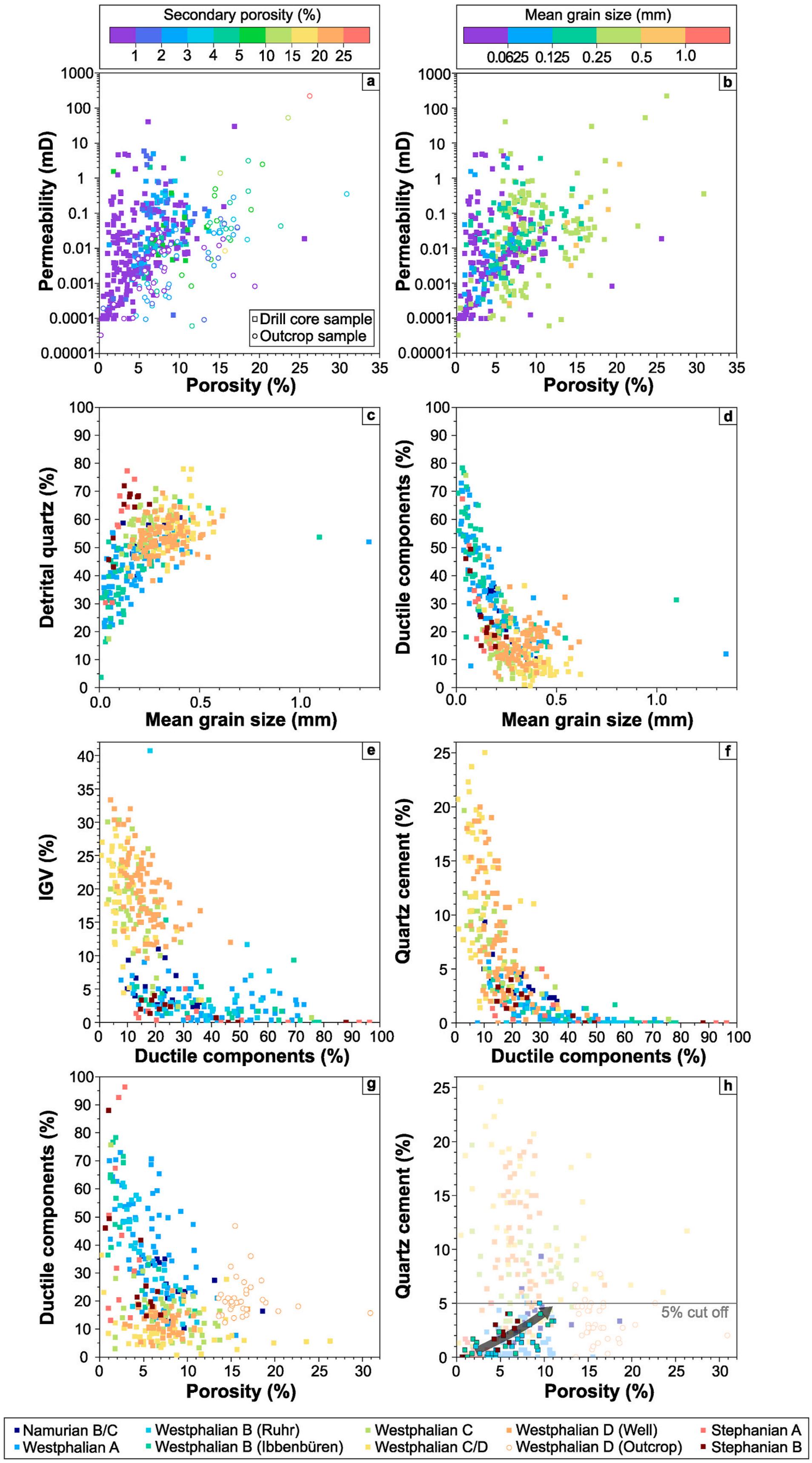

(caption on next page)

Fig. 6. (a) Correlations of petrophysical and petrographical data. (a) Porosity-permeability plot with secondary porosity indicated by color code and subdivided into drill core and outcrop samples. (b) Porosity-permeability plot with grain size indicated by color code. (c) Detrital quartz ($R^2 = 0.3$) and (d) ductile component contents ($R^2 = 0.4$) plotted against mean grain size. (e) IGV ($R^2 = 0.5$) and (f) quartz cement content ($R^2 = 0.4$) plotted against ductile component content. (g) Ductile component ($R^2 = 0.2$) and (h) quartz cement contents plotted against porosity. Gray arrow indicates positive correlations ($R^2 > 0.5$) between quartz cement and porosity for Westphalian B (Ruhr), Westphalian B (Ibbenbüren), and Stephanian B samples that are characterized by quartz cement contents <5%. Data were compiled from literature (Becker et al., 2017; Wüstefeld et al., 2017a; Busch et al., 2019; Quandt et al., 2022a, accepted; Greve et al., 2023, 2024, under review) and complemented by new data.

Due to this compositional similarity, potential changes in source area cannot be inferred from the petrographic data presented here. Additionally, heavy mineral contents do not show systematic variations over time (Fig. 4c) arguing against changing source areas. Individual peaks in igneous rock fragment contents (Fig. 2j) might indicate higher input from the igneous rocks in the Harz mountains relative to Rhenish massif and Baltica-derived clastics. The Pennine basin located in the western Variscan foreland and separated from the Ruhr foreland basin by the London-Brabant high (Cleal et al., 2009) shows an additional northern sediment source, which may be eastern Greenland and/or western Scandinavia (e.g. Hallsworth et al., 2000; Morton et al., 2001; Morton and Whitham, 2002). Sediment was probably transported southward along the proto-Viking graben (Haszeldine, 1984; Morton et al., 2001; Morton and Whitham, 2002). Uplift and erosion in the north had an immediate effect on deposition in the south (Critelli and Reed, 1999; Morton and Whitham, 2002). Despite this regional geological effect, a northern source area has not been demonstrated for the Variscan Ruhr and Lower Saxony foreland basins and the siliciclastic rocks analyzed here lack high-grade metasedimentary components as observed in the Pennine basin and associated with a northern source (Hallsworth et al., 2000; Morton et al., 2001; Morton and Whitham, 2002).

5.1.3. Variations in transport distance

The transport distance from source to sink area may have varied over time as a result of the northwestward migrating Variscan front (Shackleton et al., 1982; Ahrendt et al., 1983). Decreasing detrital feldspar contents over time (Fig. 2e) may therefore be related to longer transport and/or residence times during which unstable feldspar dissolved. However, this interpretation contrasts increasing mean grain size over time (Fig. 2a), which rather reflect shorter transport distance due to decreasing energetic environments from source to sink. Such a negative relationship between grain size and detrital feldspar content represents a typical observation of sandstones (Odom, 1975).

5.1.4. Sediment recycling

Repeated reworking and recycling of sedimentary rocks generally produce better sorted, negatively skewed sediments rich in stable quartz and poor in unstable components like feldspar, feldspar-bearing igneous rock fragments, and some heavy minerals except for stable zircon, tourmaline, and rutile. Most Westphalian C-D samples meet these criteria (Fig. 2b–e, j). Additionally, sediment recycling has been previously suggested in order to explain Baltica-derived zircons (Franke and Dulce, 2017; Franke et al., 2019) and is consistent with the winnowing process inferred from trends in mean grain size, sorting, and skewness (Fig. 2a–c).

5.1.5. Synthesis

Taken together, the petrographic changes over time and especially along the Westphalian B–C boundary may be explained by a combination of unroofing and sediment recycling. Observations that are not in agreement with unroofing (e.g. decreasing feldspar content, lack of any systematic variation in heavy mineral content), may be explained by recycling during which unstable components became progressively dissolved. This model temporally coincides with regional Westphalian C-D tectonic pulses such as the pre-Leonian and Malvernian phases during which the Variscan hinterland was uplifted (Cleal et al., 2009).

5.2. Implications of basin-specific burial and uplift history

Each basin is characterized by a distinctive burial and uplift history (Littke et al., 1994, 2000; Bruns et al., 2013, Greve et al. in review and references therein, Fig. 7). During the first burial phase in Late Carboniferous to Early Permian, the sedimentary infill of the Ruhr foreland basin and Saar-Nahe intramontane basin reached their maximum burial depths. Subsequent Permian uplift affected all basins and exposed Upper Carboniferous strata from the Ruhr and Lower Saxony basin to the surface. The second burial phase beginning in Late Permian-Early Triassic is particularly pronounced in the Lower Saxony basin where the maximum burial depth was achieved in mid-Cretaceous times. Simultaneously, the Ruhr and Saar-Nahe basin experienced renewed Cretaceous uplift with the former being exposed to the surface. A third subordinate burial phase from mid Cretaceous to Late Paleogene is restricted to the Ruhr basin.

Previously published paleogeothermal gradients for the study areas are controversial and range from 36 to 47 °C/km (Littke et al., 1994, 2000; Senglaub et al., 2006) to up to 92 °C/km (Buntebarth et al., 1982) at the respective time of maximum burial. The lower end of this range covers typical geothermal gradients (<50 °C/km) of recent foreland basins, whereas the upper range significantly exceeds them (Kolawole and Evenick, 2023). The paleogeothermal gradients of the Ruhr (36–47 °C/km), Lower Saxony (43–47 °C/km), and Saar-Nahe basins (approximately 45 °C/km) at the respective time of maximum burial proposed in more recent publications (Littke et al., 1994, 2000; Senglaub et al., 2006) overlap. Consequently, by assuming a consistent geothermal gradient of 45 °C/km for all study areas at the respective time of maximum burial, Westphalian A-D sedimentary rocks of the Saar-Nahe, Lower Saxony, and Ruhr basin reached peak burial temperatures of 300, 270 °C, and 200 °C, respectively (Fig. 7).

According to the basin-specific paleogeothermal gradients, burial, and uplift paths, distinct diagenetic sequences have been proposed (Becker et al., 2017, Wüstefeld et al., 2017a, Busch et al., 2019, Quandt et al., 2022a, accepted, Greve et al., 2023, 2024, under review, Fig. 7). Accordingly, dissolution of detrital and authigenic components has been similarly attributed to the first burial and subsequent uplift phases. The respective burials are accompanied by mechanical compaction. During the respective first burial phase, quartz cementation took place indicating that temperatures between 75 and 165 °C (Walderhaug 1994) were reached in all basins studied.

Further quartz cementation is extensively recorded in Westphalian C-D rocks of the Lower Saxony basin (Fig. 4e). As all basins reached temperature conditions suitable for quartz cementation, this difference in quartz cement content may be related to longer residence times of the Lower Saxony Westphalian C-D sediment package in the temperature range 75–165 °C. In addition, the trend of quartz cement content over time (Fig. 4e) mimics the mean grain size trend (Fig. 2a), and large grain sizes favor quartz cementation (Lander et al., 2008; Prajapati et al., 2020). However, no clear positive correlation between quartz cement and mean grain size is observed here.

Instead, quartz cement and ductile component contents reveal opposing trends over time (Fig. 4b–e), and Lower Saxony Westphalian C-D samples show the highest quartz cement and lowest ductile component contents. This observation is in accordance with COPL and CEPL trends (Fig. 5d and e). Indeed, the porosity loss of the whole sample set is dominated by mechanical compaction, but especially Westphalian C-D samples from the Lower Saxony basin are shifted toward ICOMPACT

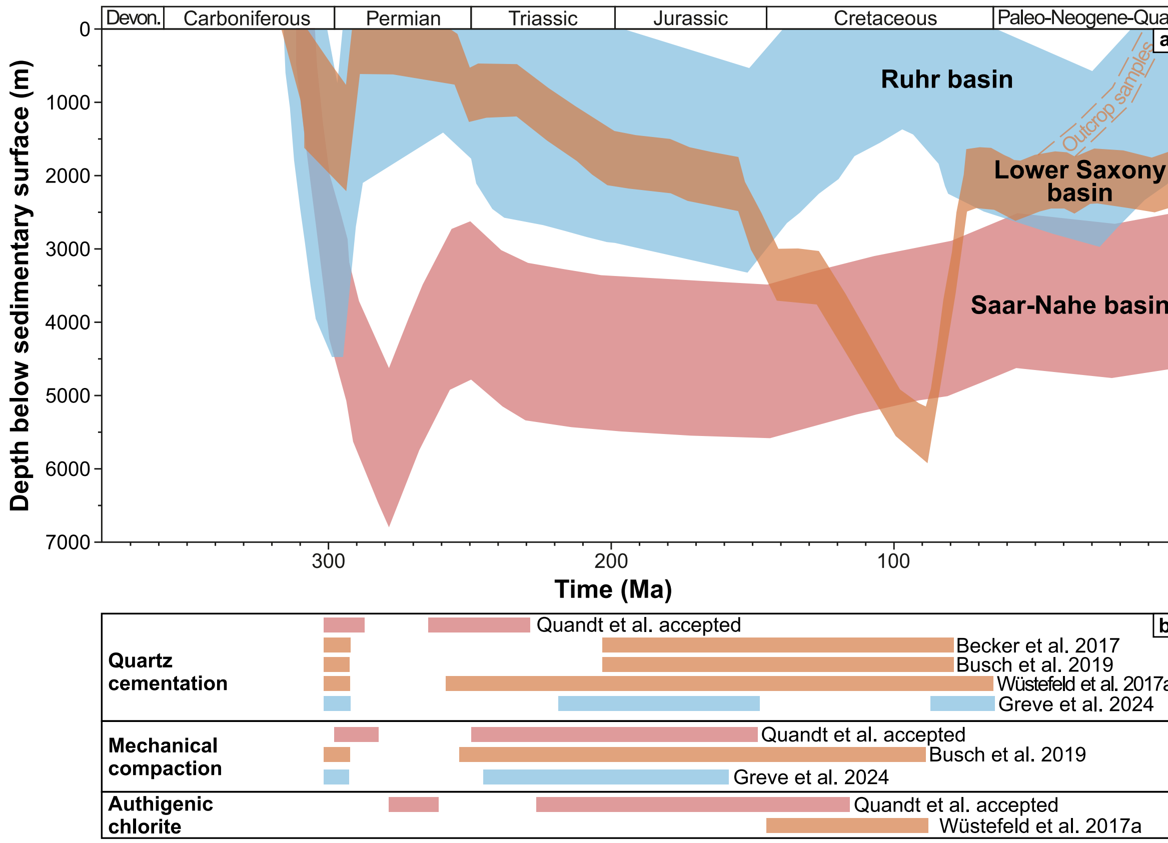

Fig. 7. (a) Schematic burial and uplift history of the basins studied (modified after Littke et al., 2000; Bruns et al., 2013; Becker et al., 2017, and Greve et al. in review). (b) Respective diagenetic sequences compiled from literature (Becker et al., 2017; Wüstefeld et al., 2017a; Busch et al., 2019; Quandt et al., accepted; Greve et al., 2024). For reasons of comparison between the different study areas, lower and upper limits of burial curves consistently refer to the respective lower Westphalian A and upper Westphalian D boundary.

values < 0.5 implying an increasing influence of cementational porosity loss (Fig. 5f). This may be related to higher peak temperatures that these rocks reached in comparison with the Ruhr basin. A thermal effect on sandstone compaction behavior has been observed previously (Trevena and Clark, 1986; Lundegard and Trevena, 1990; Lundegard, 1992 and references therein). Accordingly, higher temperatures promote the onset of diagenetic reactions and increase their rates. However, this temperature effect is not reflected by porosity and permeability data due to the effect of surface weathering, dissolution, and formation of secondary porosity.

Similarly, authigenic chlorite may form in sandstones on the expense of carbonate and clay minerals at temperatures as low as >60 °C to up to >120 °C (Worden et al., 2020 and references therein). Samples from the Lower Saxony basin show the highest authigenic chlorite contents (Fig. 4h). They were associated with fault-related hydrothermal (>250 °C) activity (Wüstefeld et al. 2017a, b). These fault-related temperature conditions exceed the maximum burial temperatures of 200 °C for the Ruhr basin calculated in this study and thus explain the comparatively high authigenic chlorite contents in the Lower Saxony basin. Similarly, the Saar-Nahe basin was affected by Early Rotliegend igneous activity during the volcanic syn-rift phase following the onset of burial of the Upper Carboniferous basin fill (Lorenz and Haneke, 2004; von Seckendorff et al., 2004). Interactions between igneous activity and sediments such as phreatomagmatic eruptions and contact metamorphism are described in literature (Lorenz and Haneke, 2004). However, the samples studied here (Quandt et al., accepted) do not indicate contact metamorphism. This may be related to localized igneous activity that focused along faults in the Saar-Nahe basin (Stollhofen and Stanistreet, 1994; Lorenz and Haneke, 2004). Thus, it remains unclear if the elevated authigenic chlorite contents in the samples from the Saar-Nahe basin compared to samples from the Ruhr basin are due to deeper burial and/or igneous activity.

5.3. Evolution and controlling factors of porosity and permeability

73% of the samples are classified as tight (i.e. porosity <10% and permeability <1 mD). The correlations of reservoir quality with petrographic features observed in the original publications (Becker et al., 2017; Wüstefeld et al., 2017a; Busch et al., 2019; Quandt et al., 2022a, accepted, Greve et al., 2023, 2024, under review) become vague when the samples from different localities with specific porosity and permeability values ranging over six orders of magnitude are plotted together. Nevertheless, secondary porosity and mean grain size show correlations with porosity that are valid for the whole data set (Fig. 6a and b). Secondary porosity and mean grain size are therefore the main porosity controlling factors. Reservoir quality is enhanced by 5–10 percentage points due to dissolution of unstable components. This is mainly due to surface exposure and weathering, but also affects subsurface samples (Fig. 6a).

With increasing grain size, the detrital quartz contents increase and ductile component contents decrease (Fig. 6c and d). During mechanical compaction, phyllosilicates and phyllosilicate-bearing rock fragments deformed ductile and were squeezed into pore space reducing IGV and porosity (Fig. 6e–g). However, samples rich in rigid quartz (i.e. large mean grain sizes, Fig. 6c) resisted mechanical compaction and thus preserved porosity (Fig. 6b). With an increase in detrital quartz content (Fig. 2d) and decrease in ductile component content (Fig. 4b) from the Westphalian C onwards, mechanical compaction does not efficiently reduce porosity by ductile deforming phyllosilicates. Instead, porosity loss due to cementation gains influence relative to mechanical compaction from the Westphalian C onwards. This explains the trends in COPL, CEPL, and ICOMPACT over time (Fig. 5d–f).

Furthermore, mechanical compaction may induce pressure solution initiating syntaxial quartz cement growth especially where quartz is in contact with clay minerals (Bjørlykke and Jahren, 2012). This may be indicated by similar trends in authigenic quartz and clay cement contents that are highest in Westphalian C-D samples (Fig. 4e and f).

Westphalian B (Ruhr and Ibbenbüren) and Stephanian B samples have quartz cement contents <5% and are positively correlated with porosity (Fig. 6h). All other samples (Namurian B/C, Westphalian A, Stephanian A) have similar or higher quartz cement contents (Westphalian C-D) and consistently lack any correlation with porosity (Figs. 4e and 6h). This indicates that low quartz cement contents <5% may preserve porosity by stabilizing the granular framework acting

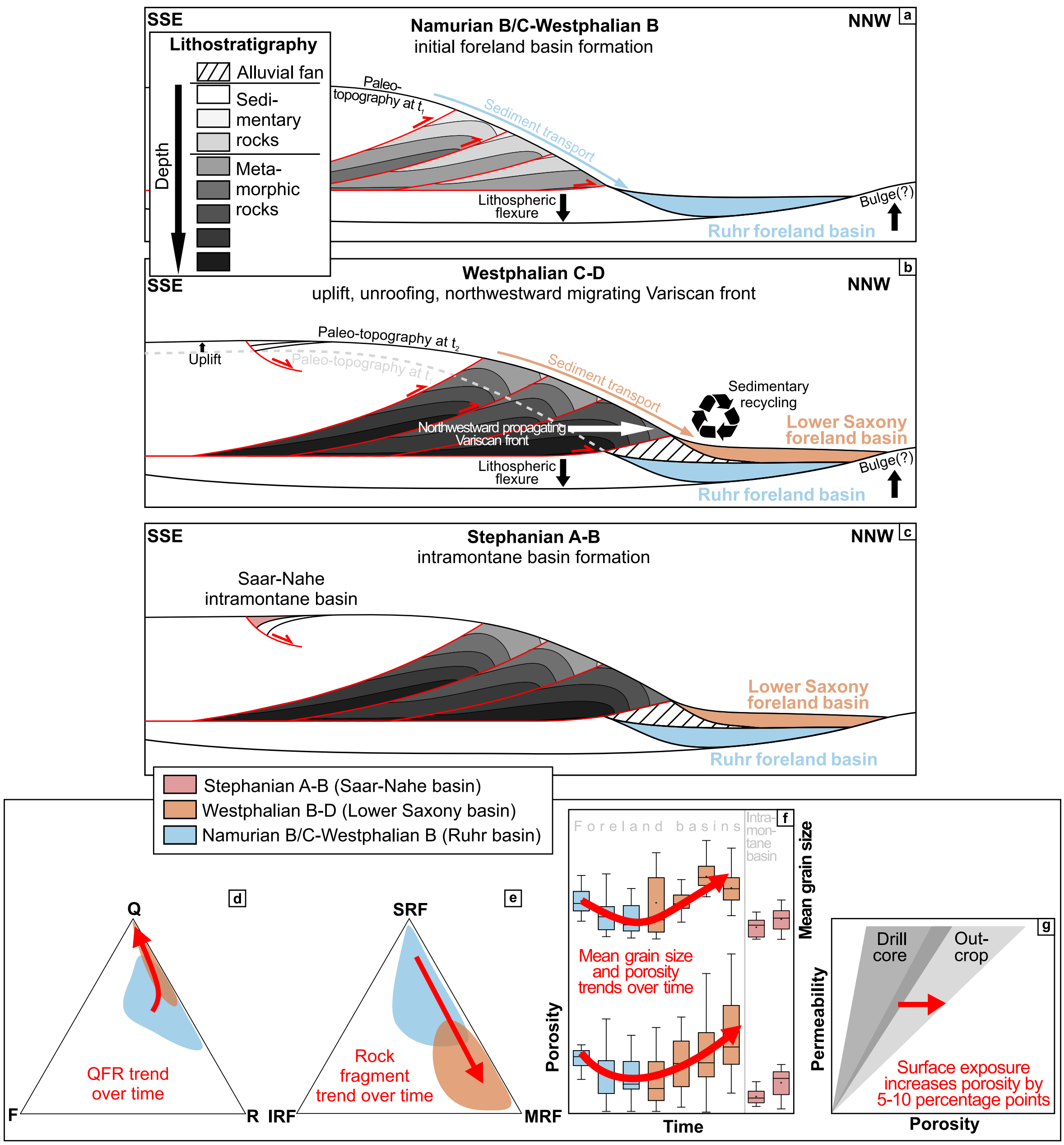

Fig. 8. Model of the tectono-sedimentary and reservoir evolution of the Variscan foreland and intramontane basins in three time steps along simplified NNW-SSE cross sections (adapted from Meissner et al., 1981). (a) In Namurian B/C to Westphalian B times, the load of the Variscan fold and thrust belt induces lithospheric flexure (e.g. Opluštil and Cleal, 2007). This initiates the formation of the Variscan foreland basin, which is filled by sediments from the Variscan hinterland (Franke and Dulce, 2017; Franke et al., 2019). (b) Northwestward propagation of the Variscan fold and thrust belt (e.g. Drozdzewski, 1993) and hinterland uplift probably in the course of the Pre-Leonian and/or Malvernian deformation phases (Jones and Glover, 2005, Cleal et al., 2009) progressively expose deeper, metamorphic rocks to the surface in Westphalian C-D times. Simultaneously, sedimentary recycling additionally increases sediment maturity. In contrast to the Variscan foreland, (c) the formation of the intramontane Saar-Nahe basin is controlled by faults forming a half-graben structure (adapted after Henk, 1993). As a result of these tectono-sedimentary processes, the sedimentary rock succession of the foreland basin reveals distinct petrographic and petrophysical trends. (d) Samples become quartz-richer (Q), while feldspar (F) and rock fragment (R) contents decrease over time (red arrow, see also Fig. 2d). (e) The proportion of metamorphic (MRF) to sedimentary rock fragments (SRF) increases over time (red arrow), whereas variations in igneous rock fragments (IRF) are insignificant (see also Fig. 3c). (f) Porosity increases over time and is controlled by mean grain size, which shows a similar increasing trend over time, and secondary porosity. (g) Surface exposure and weathering intensify secondary porosity and thus increase porosity by 5–10 percentage points.

against mechanical compaction. However, with increasing quartz cement content >5% the beneficial effect of porosity preservation diminishes and quartz cements increasingly occupy pore spaces reducing porosity. Accordingly, 5% quartz cement content marks the turning point between porosity enhancing and deteriorating effect within this samples set.

6. Conclusions

The comprehensive data compilation covering Namurian B/C to Westphalian D foreland basin siliciclastic rocks provides insights into the Variscan foreland evolution from source to sink to burial and uplift (Fig. 8). The Westphalian B–C boundary marks an increase in grain size and sorting, detrital quartz content, proportion of metamorphic to sedimentary rock fragment content, quartz cement content, primary and secondary porosity, a change in type of porosity loss (COPL vs. CEPL), and a decrease in detrital feldspar and rock fragment contents. These petrographic and petrophysical changes are temporally and causally in accordance with late Westphalian tectonic uplift phases (pre-Leonian and/or Malvernian) and associated unroofing of the hinterland and sedimentary recycling in the course of northwestward propagating Variscan fold and thrust belt. Thus, tectonics have a greater influence on sandstone petrography than the depositional environment.

Evolution of porosity and permeability of the predominantly tight siliciclastic rocks (73% of the samples have a porosity <10% and a permeability <1 mD) are mainly controlled by grain size and secondary porosity. With increasing grain size and weathering of rocks exposed to the surface, porosity increases. Accordingly, Westphalian C-D samples show the highest porosity values (up to 31%). They are also characterized by the lowest ductile component contents. During mechanical compaction ductile behaving components reduce IGV and porosity.

Basin-specific burial paths with characteristic maximum burial temperatures increased the proportion of cementational porosity loss. This temperature effect on diagenesis is reflected by high quartz cement contents up to 25% and authigenic chlorite occurrences among the samples from the Lower Saxony basin that experienced a higher maximum burial temperature than the Ruhr basin and was additionally affected by local fault-related hydrothermal activity. A quartz cement content of 5% marks the turning from potentially reservoir enhancing to reservoir deteriorating effects.

CRediT authorship contribution statement

Dennis Quandt: Writing – review & editing, Writing – original draft, Visualization, Project administration, Investigation, Formal analysis, Conceptualization. **Benjamin Busch:** Writing – review & editing, Resources, Methodology, Funding acquisition. **Christoph Hilgers:** Writing – review & editing, Funding acquisition.

Declaration of competing interest

The authors declare that they have no known competing financial interests or personal relationships that could have appeared to influence the work reported in this paper.

Data availability

Data used in this study are provided in the supplementary material.

Acknowledgements

This study was carried out in the framework of the project FloodRisk that was funded by the German Federal Ministry of Education and Research (FKZ 03G0893A). We thank Sara Criniti and Graham Blackbourn for their constructive comments and Salvatore Critelli for editorial handling.

Appendix A. Supplementary data

Supplementary data to this article can be found online at https://doi.org/10.1016/j.marpetgeo.2024.106774.

References

Ahrendt, H., Clauer, N., Hunziker, J.C., Weber, K., 1983. Migration of folding and metamorphism in the Rheinische Schiefergebirge deduced from K-Ar and Rb-Sr age determinations. In: Martin, H., Eder, F.M. (Eds.), Intracontinental Fold Belts, Case Studies in the Variscan Belt of Europe and the Damara Belt in Namibia. Springer, Berlin, Heidelberg, pp. 323–338. https://doi.org/10.1007/978-3-642-69124-9_15.

Allen, P.A., Homewood, P., 1986. Foreland Basins, vol. 8. International Association of Sedimentologists Special Publication, pp. 1–457. https://doi.org/10.1002/9781444303810.

Banks, J., Harris, N.B., 2018. Geothermal potential of foreland basins: a case study from the western Canadian sedimentary basin. Geothermics 76, 74–92. https://doi.org/10.1016/j.geothermics.2018.06.004.

Becker, I., Wüstefeld, P., Koehrer, B., Felder, M., Hilgers, C., 2017. Porosity and permeability variations in a tight gas sandstone reservoir analogue, Westphalian D, Lower Saxony Basin, NW Germany: influence of depositional setting and diagenesis. J. Petrol. Geol. 40 (4), 363–389. https://doi.org/10.1111/jpg.12685.

Behr, H.J., Engel, W., Franke, W., Giese, P., Weber, K., 1984. The Variscan belt in Central Europe: main structures, geodynamic implications, open questions. Tectonophysics 109 (1–2), 15–40. https://doi.org/10.1016/0040-1951(84)90168-9.

Bjørlykke, K., Jahren, J., 2012. Open or closed geochemical systems during diagenesis in sedimentary basins: constraints on mass transfer during diagenesis and the prediction of porosity in sandstone and carbonate reservoirs. AAPG Bull. 96 (12), 2193–2214. https://doi.org/10.1306/04301211139.

Bruns, B., Di Primio, R., Berner, U., Littke, R., 2013. Petroleum system evolution in the inverted Lower Saxony Basin, northwest Germany: a 3 D basin modeling study. Geofluids 13 (2), 246–271. https://doi.org/10.1111/gfl.12016.

Buntebarth, G., Koppe, I., Teichmüller, M., 1982. Palaeogeothermics in the Ruhr basin. In: Cermak, V., Haenel, R. (Eds.), Geothermics and Geothermal Energy. Schweizerbart, Stuttgart, pp. 45–55.

Busch, B., Becker, I., Koehrer, B., Adelmann, D., Hilgers, C., 2019. Porosity evolution of two Upper Carboniferous tight-gas-fluvial sandstone reservoirs: impact of fractures and total cement volumes on reservoir quality. Mar. Petrol. Geol. 100, 376–390. https://doi.org/10.1016/j.marpetgeo.2018.10.051.

Civitelli, M., Critelli, S., Ingersoll, R.V., 2024. Interpreting post-depositional alterations in deep-marine sandstones: butano Sandstone, central California USA. Mar. Petrol. Geol., 106733 https://doi.org/10.1016/j.marpetgeo.2024.106733.

Civitelli, M., Ravidà, D.C., Borrelli, M., Criniti, S., Falsetta, E., 2023. Diagenesis and petrophysics of Miocene sandstones within southern Apennines foreland, Italy. Mar. Petrol. Geol. 155, 106411 https://doi.org/10.1016/j.marpetgeo.2023.106411.

Cleal C, J., Opluštil, S., Thomas, B.A., Tenchov, Y., Abbink, O.A., Bek, J., Dimitrova, T., Drábková, J., Hartkopf-Fröder, C., van Hoof, T., Kędzior, A., Jarzembowski, E., Jasper, K., Libertin, M., McLean, D., Oliwkiewicz-Miklasinska, M., Pšenička, J., Ptak, B., Schneider, J.W., Schultka, S., Šimůnek, Z., Uhl, D., Waksmundzka, M.I., van Waveren, I., Zodrow, E.L., 2009. Late moscovian terrestrial biotas and palaeoenvironments of variscan euramerica. Neth. J. Geosci. 88 (4), 181–278. https://doi.org/10.1017/S0016774600000846.

Corfield, S.M., Gawthorpe, R.L., Gage, M., Fraser, A.J., Besly, B.M., 1996. Inversion tectonics of the variscan foreland of the British isles. J. Geol. Soc. 153 (1), 17–32. https://doi.org/10.1144/gsjgs.153.1.0017.

Costamagna, L.G., Criniti, S., 2024. Interpreting siliciclastic sedimentation in the upper paleozoic mulargia-escalaplano basin (sardinia, Italy): influence of tectonics on provenance. J. Palaeogeogr. 13 (1), 18–34. https://doi.org/10.1016/j.jop.2023.10.005.

Criniti, S., Martín-Martín, M., Martín-Algarra, A., 2023. New constraints for the western paleotethys paleogeography-paleotectonics derived from detrital signatures: malaguide carboniferous culm cycle (betic cordillera, S Spain). Sediment. Geol. 458, 106534 https://doi.org/10.1016/j.sedgeo.2023.106534.

Critelli, S., 2018. Provenance of Mesozoic to Cenozoic circum-Mediterranean sandstones in relation to tectonic setting. Earth Sci. Rev. 185, 624–648. https://doi.org/10.1016/j.earscirev.2018.07.001.

Critelli, S., Criniti, S., 2021. Sandstone petrology and provenance in fold thrust belt and foreland basin system. In: Al-Juboury, A.I. (Ed.), Sedimentary Petrology - Implications in Petroleum Industry, vol. 9. Intech Open Access Publisher, Janeza Trdine, Rijeka, Croatia, pp. 1–15. https://doi.org/10.5772/intechopen.96985.

Critelli, S., Criniti, S., Ingersoll, R.V., Cavazza, W., 2023. Temporal and spatial significance of volcanic particles in sand (stone): implications for provenance and palaeotectonic reconstructions. Geological Society, London, Special Publications 520 (1), 311–325. https://doi.org/10.1144/SP520-2022-99.

Critelli, S., Le Pera, E., 1994. Detrital modes and provenance of Miocene sandstones and modern sands to the Southern Apennines thrust-top basins (Italy). J. Sediment. Res. 64 (4a), 824–835. https://doi.org/10.1306/D4267ED8-2B26-11D7-8648000102C1865D.

Critelli, S., Reed, W.E., 1999. Provenance and stratigraphy of the devonian (old red sandstone) and carboniferous sandstones of spitsbergen. Svalbard. European Journal of Mineralogy 11, 149–166. https://doi.org/10.1127/ejm/11/1/0149.

David, C., Wong, T.F., Zhu, W., Zhang, J., 1994. Laboratory measurement of compaction-induced permeability change in porous rocks: implications for the generation and

maintenance of pore pressure excess in the crust. Pure Appl. Geophys. 143 (1), 425–456. https://doi.org/10.1007/BF00874337.
DeCelles, P.G., Kapp, P., Gehrels, G.E., Ding, L., 2014. Paleocene-Eocene foreland basin evolution in the Himalaya of southern Tibet and Nepal: implications for the age of initial India-Asia collision. Tectonics 33 (5), 824–849. https://doi.org/10.1002/2014TC003522.
Dickinson, W.R., Suczek, C.A., 1979. Plate tectonics and sandstone compositions. AAPG (Am. Assoc. Pet. Geol.) Bull. 63 (12), 2164–2182. https://doi.org/10.1306/2F9188FB-16CE-11D7-8645000102C1865D.
Dorsey, R.J., 1988. Provenance evolution and unroofing history of a modern arc-continent collision; evidence from petrography of Plio-Pleistocene sandstones, eastern Taiwan. J. Sediment. Res. 58 (2), 208–218. https://doi.org/10.1306/212F8D5A-2B24-11D7-8648000102C1865D.
Drozdzewski, G., 1993. The Ruhr coal basin (Germany): structural evolution of an autochthonous foreland basin. Int. J. Coal Geol. 23 (1–4), 231–250. https://doi.org/10.1016/0166-5162(93)90050-K.
Duane, D.B., 1964. Significance of skewness in recent sediments, western Pamlico Sound, North Carolina. J. Sediment. Res. 34 (4), 864–874. https://doi.org/10.1306/74D711B8-2B21-11D7-8648000102C1865D.
Dusséaux, C., Gébelin, A., Ruffet, G., Mulch, A., 2021. Late carboniferous paleoelevation of the variscan belt of western Europe. Earth Planet Sci. Lett. 569, 117064 https://doi.org/10.1016/j.epsl.2021.117064.
Edlmann, K., Edwards, M.A., Qiao, X.J., Haszeldine, R.S., McDermott, C.I., 2015. Appraisal of global CO_2 storage opportunities using the geomechanical facies approach. Environ. Earth Sci. 73, 8075–8096. https://doi.org/10.1007/s12665-014-3965-3.
Folk, R.L., 1980. Petrology of Sedimentary Rocks. Hemphill Publishing Company, Austin.
Folk, R.L., Ward, W.C., 1957. Brazos River bar [Texas], a study in the significance of grain size parameters. J. Sediment. Res. 27 (1), 3–26. https://doi.org/10.1306/74D70646-2B21-11D7-8648000102C1865D.
Franke, W., Dulce, J.C., 2017. Back to sender: tectonic accretion and recycling of Baltica-derived Devonian clastic sediments in the Rheno-Hercynian Variscides. Int. J. Earth Sci. 106 (1), 377–386. https://doi.org/10.1007/s00531-016-1408-y.
Franke, W., Huckriede, H., O'Sullivan, P., Wemmer, K., 2019. Zircons to the front: accretionary history of the Rheno-Hercynian active margin (Variscides, Germany). Can. J. Earth Sci. 56 (12), 1375–1397. https://doi.org/10.1139/cjes-2018-0255.
Friedman, G.M., 1961. Distinction between dune, beach, and river sands from their textural characteristics. J. Sediment. Res. 31 (4), 514–529. https://doi.org/10.1306/74D70BCD-2B21-11D7-8648000102C1865D.
Garzanti, E., 2016. From static to dynamic provenance analysis—sedimentary petrology upgraded. Sediment. Geol. 336, 3–13. https://doi.org/10.1016/j.sedgeo.2015.07.010.
Garzanti, E., 2019. Petrographic classification of sand and sandstone. Earth Sci. Rev. 192, 545–563. https://doi.org/10.1016/j.earscirev.2018.12.014.
Garzanti, E., Andò, S., Vezzoli, G., 2006. The continental crust as a source of sand (Southern Alps cross section, northern Italy). J. Geol. 114 (5), 533–554. https://doi.org/10.1086/506159.
Garzanti, E., Vezzoli, G., Lombardo, B., Ando, S., Mauri, E., Monguzzi, S., Russo, M., 2004. Collision-orogen provenance (western Alps): detrital signatures and unroofing trends. J. Geol. 112 (2), 145–164. https://doi.org/10.1086/381655.
Greve, J., Busch, B., Quandt, D., Knaak, M., Hartkopf-Fröder, C., Hilgers, C., 2023. Coupling heat conductivity and lithofacies of the coal-bearing Upper Carboniferous in the eastern Ruhr Basin, NW Germany. Z. Dtsch. Ges. Geowiss. 173 (4), 673–695. https://doi.org/10.1127/zdgg/2023/0350.
Greve, J., Busch, B., Quandt, D., Knaak, M., Hilgers, C., 2024. The influence of sedimentary facies, mineralogy, and diagenesis on reservoir properties of the coal-bearing Upper Carboniferous of NW Germany. Petrol. Geosci. 30 (1) https://doi.org/10.1144/petgeo2023-020 petgeo2023-020.
Greve, J., Busch, B., Quandt, D., Knaak, M., Hilgers, C., Under review. Understanding the interplay of sedimentary facies, mineralogy, and diagenesis on reservoir properties of the coal-bearing Upper Carboniferous Westphalian A and B of the Ruhr Area, NW Germany. Under review in Int. J. Earth Sci...
Hallsworth, C.R., Morton, A.C., Claoué-Long, J., Fanning, C.M., 2000. Carboniferous sand provenance in the Pennine Basin, UK: constraints from heavy mineral and detrital zircon age data. Sediment. Geol. 137 (3–4), 147–185. https://doi.org/10.1016/S0037-0738(00)00153-6.
Haszeldine, R.S., 1984. Carboniferous North Atlantic palaeogeography: stratigraphic evidence for rifting, not megashear or subduction. Geol. Mag. 121 (5), 443–463. https://doi.org/10.1017/S0016756800029988.
Henk, A., 1993. Late orogenic basin evolution in the variscan internides: the Saar-Nahe basin, southwest Germany. Tectonophysics 223 (3–4), 273–290. https://doi.org/10.1016/0040-1951(93)90141-6.
Jones, N.S., Glover, B.W., 2005. Fluvial sandbody architecture, cyclicity and sequence stratigraphical setting–implications for hydrocarbon reservoirs: the Westphalian C and D of the Osnabrück-Ibbenbüren area, northwest Germany. In: Collinson, J.D., Evans, D.J., Holliday, D.W., Jones, N.S. (Eds.), Carboniferous Hydrocarbon Resources: the Southern North Sea and Surrounding Onshore Areas, vol. 7. Yorkshire Geological Society, pp. 57–74.
Khan, S.H., Sheng, Y.M., Critelli, S., Civitelli, M., Mughal, M.S., Basharat, U., 2024. Depositional and diagenetic controls on reservoir properties of the lower Cambrian Khewra Sandstone, eastern salt range, Sub-Himalaya, Pakistan. Mar. Petrol. Geol. 161, 106651 https://doi.org/10.1016/j.marpetgeo.2023.106651.
Klinkenberg, L.J., 1941. The Permeability of Porous Media to Liquids and Gases. Drilling and Production Practice. American Petroleum Institute, Washington, D.C., pp. 200–213
Kolawole, F., Evenick, J.C., 2023. Global distribution of geothermal gradients in sedimentary basins. Geosci. Front. 14 (6), 101685 https://doi.org/10.1016/j.gsf.2023.101685.
Korsch, R.J., Schäfer, A., 1991. Geological interpretation of DEKORP deep seismic reflection profiles 1C and 9N across the variscan Saar-Nahe Basin southwest Germany. Tectonophysics 191 (1–2), 127–146. https://doi.org/10.1016/0040-1951(91)90236-L.
Korsch, R.J., Schäfer, A., 1995. The Permo-Carboniferous Saar-Nahe Basin, south-west Germany and north-east France: basin formation and deformation in a strike-slip regime. Geol. Rundsch. 84 (2), 293–318. https://doi.org/10.1007/BF00260442.
Lander, R.H., Larese, R.E., Bonnell, L.M., 2008. Toward more accurate quartz cement models: the importance of euhedral versus noneuhedral growth rates. AAPG Bull. 92 (11), 1537–1563. https://doi.org/10.1306/07160808037.
Littke, R., Büker, C., Lückge, A., Sachsenhofer, R.F., Welte, D.H., 1994. A new evaluation of palaeo-heat flows and eroded thicknesses for the Carboniferous Ruhr basin, western Germany. Int. J. Coal Geol. 26 (3–4), 155–183. https://doi.org/10.1016/0166-5162(94)90009-4.
Littke, R., Büker, C., Hertle, M., Karg, H., Stroetmann-Heinen, V., Oncken, O., 2000. Heat flow evolution, subsidence and erosion in the Rheno-Hercynian orogenic wedge of central Europe. Geological Society, London, Special Publications 179 (1), 231–255. https://doi.org/10.1144/GSL.SP.2000.179.01.15.
Lorenz, V., Haneke, J., 2004. Relationship between diatremes, dykes, sills, laccoliths, intrusive-extrusive domes, lava flows, and tephra deposits with unconsolidated water-saturated sediments in the late Variscan intermontane Saar-Nahe Basin, SW Germany. Geological Society, London, Special Publications 234 (1), 75–124. https://doi.org/10.1144/GSL.SP.2004.234.01.07.
Lucas, S.G., Schneider, J.W., Nikolaeva, S., Wang, X., 2022. The Carboniferous timescale: an introduction. Geological Society, London, Special Publications 512 (1), 1–17. https://doi.org/10.1144/SP512-2021-160.
Lundegard, P.D., 1992. Sandstone porosity loss; a" big picture" view of the importance of compaction. J. Sediment. Res. 62 (2), 250–260. https://doi.org/10.1306/D42678D4-2B26-11D7-8648000102C1865D.
Lundegard, P.D., Trevena, A.S., 1990. Sandstone diagenesis in the Pattani Basin (Gulf of Thailand): history of water-rock interaction and comparison with the Gulf of Mexico. Appl. Geochem. 5 (5–6), 669–685. https://doi.org/10.1016/0883-2927(90)90064-C.
Mack, G.H., 1984. Exceptions to the relationship between plate tectonics and sandstone composition. J. Sediment. Res. 54 (1), 212–220. https://doi.org/10.1306/212F83E6-2B24-11D7-8648000102C1865D.
Mann, P., Gahagan, L., Gordon, M.B., 2003. Tectonic setting of the world's giant oil and gas fields. In: Halbouty, M.T. (Ed.), Giant Oil and Gas Fields of the Decade 1990–1999, vol. 78. AAPG Memoir, pp. 15–105.
Matte, P., 2001. The Variscan collage and orogeny (480–290 Ma) and the tectonic definition of the Armorica microplate: a review. Terra. Nova 13 (2), 122–128. https://doi.org/10.1046/j.1365-3121.2001.00327.x.
Maynard, J.R., Hofmann, W., Dunay, R.E., Benthan, P.N., Dean, K.P., Watson, I., 1997. The Carboniferous of Western Europe; the development of a petroleum system. Petrol. Geosci. 3 (2), 97–115. https://doi.org/10.1144/petgeo.3.2.97.
McLaren, P., 1981. An interpretation of trends in grain size measures. J. Sediment. Res. 51 (2), 611–624. https://doi.org/10.1306/212F7CF2-2B24-11D7-8648000102C1865D.
Meissner, R., Bartelsen, H., Murawski, H., 1981. Thin-skinned tectonics in the northern rhenish massif, Germany. Nature 290 (5805), 399–401. https://doi.org/10.1038/290399a0.
Morton, A.C., Claoué-Long, J.C., Hallsworth, C.R., 2001. Zircon age and heavy mineral constraints on provenance of North Sea Carboniferous sandstones. Mar. Petrol. Geol. 18 (3), 319–337. https://doi.org/10.1016/S0264-8172(00)00065-9.
Morton, A.C., Whitham, A.G., 2002. The Millstone Grit of northern England: a response to tectonic evolution of a northern sourceland. Proc. Yorks. Geol. Soc. 54 (1), 47–56. https://doi.org/10.1144/pygs.54.1.47.
Nagel, S., Castelltort, S., Garzanti, E., Lin, A.T., Willett, S.D., Mouthereau, F., Limonta, M., Adatte, T., 2014. Provenance evolution during arc–continent collision: sedimentary petrography of Miocene to Pleistocene sediments in the western foreland basin of Taiwan. J. Sediment. Res. 84 (7), 513–528. https://doi.org/10.2110/jsr.2014.44.
Nance, R.D., Gutiérrez-Alonso, G., Keppie, J.D., Linnemann, U., Murphy, J.B., Quesada, C., Strachan, R.A., Woodcock, N.H., 2010. Evolution of the Rheic ocean. Gondwana Res. 17 (2–3), 194–222. https://doi.org/10.1016/j.gr.2009.08.001.
Odom, I.E., 1975. Feldspar-grain size relations in Cambrian arenites, upper Mississippi Valley. J. Sediment. Res. 45 (3), 636–650. https://doi.org/10.1306/212F6E01-2B24-11D7-8648000102C1865D.
Oncken, O., Von Winterfeld, C., Dittmar, U., 1999. Accretion of a rifted passive margin: the Late Paleozoic Rhenohercynian fold and thrust belt (Middle European Variscides). Tectonics 18 (1), 75–91. https://doi.org/10.1029/98TC02763.
Opluštil, S., Cleal, C.J., 2007. A comparative analysis of some Late Carboniferous basins of Variscan Europe. Geol. Mag. 144 (3), 417–448. https://doi.org/10.1017/S0016756807003330.
Paxton, S.T., Szabo, J.O., Ajdukiewicz, J.M., Klimentidis, R.E., 2002. Construction of an intergranular volume compaction curve for evaluating and predicting compaction and porosity loss in rigid-grain sandstone reservoirs. AAPG Bull. 86 (12), 2047–2067.
Prajapati, N., Abad Gonzalez, A., Selzer, M., Nestler, B., Busch, B., Hilgers, C., 2020. Quartz cementation in polycrystalline sandstone: insights from phase-field simulations. J. Geophys. Res. Solid Earth 125 (2), e2019JB019137. https://doi.org/10.1029/2019JB019137.

Quandt, D., Busch, B., Fuchs, H., Alvaro de la Barrera, A., Greve, J., Hilgers, C., 2022a. Petrographical and petrophysical properties of tight siliciclastic rocks from the Ibbenbueren coal mine with regard to mine flooding. Z. Dtsch. Ges. Geowiss. 173 (4) https://doi.org/10.1127/zdgg/2022/0343.

Quandt, D., Busch, B., Greve, J., Hilgers, C., accepted. Rock characteristics and reservoir properties of Upper Carboniferous (Stephanian A-B) tight siliciclastic rocks from the Saar-Nahe basin (SW Germany). Accepted for publication in International Journal of Earth Sciences, IJES-D-23-00376..

Quandt, D., Busch, B., Schmidt, C., Hilgers, C., 2022b. Diagenesis and controls on reservoir quality of Lower Triassic red bed sandstones (Buntsandstein) from a marginal basin facies, southwest Germany. Mar. Petrol. Geol. 142, 105744 https://doi.org/10.1016/j.marpetgeo.2022.105744.

Rieckmann, M., 1970. Untersuchung von Turbulenzerscheinungen beim Fließen von Gasen durch Speichergesteine unter Berücksichtigung der Gleitströmung. Erdol Erdgas Z 86, 36–51.

Roscher, M., Schneider, J.W., 2006. Permo-Carboniferous climate: early Pennsylvanian to Late Permian climate development of central Europe in a regional and global context. Geological Society, London, Special Publications 265 (1), 95–136. https://doi.org/10.1144/GSL.SP.2006.265.01.05.

Schäfer, A., 2011. Tectonics and sedimentation in the continental strike-slip Saar-Nahe basin (Carboniferous-Permian, West Germany). Z. Dtsch. Ges. Geowiss. 162 (2), 127–155. https://doi.org/10.1127/1860-1804/2011/0162-0127.

Schäfer, A., Korsch, R.J., 1998. Formation and sediment fill of the Saar-Nahe basin (Permo-Carboniferous, Germany). Z. Dtsch. Geol. Ges. 149 (2), 233–269. https://doi.org/10.1127/zdgg/149/1998/233.

Schneider, J.W., Lucas, S.G., Scholze, F., Voigt, S., Marchetti, L., Klein, H., Opluštil, S., Werneburg, R., Golubev, V.K., Barrick, J.E., Nemyrovska, T., Ronchi, A., Day, M.O., Silantiev, V.V., Rößler, R., Saber, H., Linnemann, U., Zharinova, V., Shen, S.-Z., 2020. Late paleozoic–early mesozoic continental biostratigraphy — links to the standard global chronostratigraphic scale. Palaeoworld 29, 186–238. https://doi.org/10.1016/j.palwor.2019.09.001.

Senglaub, Y., Littke, R., Brix, M.R., 2006. Numerical modelling of burial and temperature history as an approach for an alternative interpretation of the Bramsche anomaly, Lower Saxony Basin. Int. J. Earth Sci. 95, 204–224. https://doi.org/10.1007/s00531-005-0033-y.

Shackleton, R.M., Ries, A.C., Coward, M.P., 1982. An interpretation of the Variscan structures in SW England. J. Geol. Soc. 139 (4), 533–541. https://doi.org/10.1144/gsjgs.139.4.0533.

Stollhofen, H., 1998. Facies architecture variations and seismogenic structures in the Carboniferous–Permian Saar–Nahe Basin (SW Germany): evidence for extension-related transfer fault activity. Sediment. Geol. 119 (1–2), 47–83. https://doi.org/10.1016/S0037-0738(98)00040-2.

Stollhofen, H., Stanistreet, I.G., 1994. Interaction between bimodal volcanism, fluvial sedimentation and basin development in the Permo-Carboniferous Saar-Nahe Basin (south-west Germany). Basin Res. 6 (4), 245–267. https://doi.org/10.1111/j.1365-2117.1994.tb00088.x.

Trevena, A.S., Clark, R.A., 1986. Diagenesis of sandstone reservoirs of pattani basin, gulf of Thailand. AAPG Bull. 70 (3), 299–308. https://doi.org/10.1306/9488567E-1704-11D7-8645000102C1865D.

Von Seckendorff, V., Arz, C., Lorenz, V., 2004. Magmatism of the late variscan intermontane Saar-Nahe basin (Germany): a review. Geological Society, London, Special Publications 223 (1), 361–391. https://doi.org/10.1144/GSL.SP.2004.223.01.16.

Walderhaug, O., 1994. Temperatures of quartz cementation in Jurassic sandstones from the Norwegian continental shelf; evidence from fluid inclusions. J. Sediment. Res. 64 (2a), 311–323. https://doi.org/10.1306/D4267D89-2B26-11D7-8648000102C1865D.

Worden, R.H., Armitage, P.J., Butcher, A.R., Churchill, J.M., Csoma, A.E., Hollis, C., Lander, R.H., Omma, J.E., 2018. Petroleum reservoir quality prediction: overview and contrasting approaches from sandstone and carbonate communities. Geological Society, London, Special Publications 435 (1), 1–31. https://doi.org/10.1144/SP435.21.

Worden, R.H., Griffiths, J., Wooldridge, L.J., Utley, J.E.P., Lawan, A.Y., Muhammed, D. D., Simon, N., Armitage, P.J., 2020. Chlorite in sandstones. Earth Sci. Rev. 204, 103105 https://doi.org/10.1016/j.earscirev.2020.103105.

Wüstefeld, P., Hilse, U., Koehrer, B., Adelmann, D., Hilgers, C., 2017a. Critical evaluation of an Upper Carboniferous tight gas sandstone reservoir analog: diagenesis and petrophysical aspects. Mar. Petrol. Geol. 86, 689–710. https://doi.org/10.1016/j.marpetgeo.2017.05.034.

Wüstefeld, P., Hilse, U., Lüders, V., Wemmer, K., Koehrer, B., Hilgers, C., 2017b. Kilometer-scale fault-related thermal anomalies in tight gas sandstones. Mar. Petrol. Geol. 86, 288–303. https://doi.org/10.1016/j.marpetgeo.2017.05.015.